nature communications

Article

https://doi.org/10.1038/s41467-025-58032-w

Identification of a *SNAI1* enhancer RNA that drives cancer cell plasticity

Received: 27 September 2024

Accepted: 11 March 2025

Published online: 25 March 2025

Check for updates

Chuannan Fan[1,5], Qian Wang[1,5] ✉, Peter H. L. Krijger[2], Davy Cats[3], Miriam Selle[4], Olga Khorosjutina[4], Soniya Dhanjal[4], Bernhard Schmierer[4], Hailiang Mei[3], Wouter de Laat[2] & Peter ten Dijke[1] ✉

Enhancer RNAs (eRNAs) are a pivotal class of enhancer-derived non-coding RNAs that drive gene expression. Here we identify the *SNAI1 enhancer RNA* (*SNAI1e*; *SCREEM2*) as a key activator of *SNAI1* expression and a potent enforcer of transforming growth factor-β (TGF-β)/SMAD signaling in cancer cells. *SNAI1e* depletion impairs TGF-β-induced epithelial-mesenchymal transition (EMT), migration, in vivo extravasation, stemness, and chemotherapy resistance in breast cancer cells. *SNAI1e* functions as an eRNA to *cis*-regulate *SNAI1* enhancer activity by binding to and strengthening the enrichment of the transcriptional co-activator bromodomain containing protein 4 (BRD4) at the local enhancer. *SNAI1e* selectively promotes the expression of *SNAI1*, which encodes the EMT transcription factor SNAI1. Furthermore, we reveal that SNAI1 interacts with and anchors the inhibitory SMAD7 in the nucleus, and thereby prevents TGF-β type I receptor (TβRI) polyubiquitination and proteasomal degradation. Our findings establish *SNAI1e* as a critical driver of *SNAI1* expression and TGF-β-induced cell plasticity.

Epithelial-to-mesenchymal transition (EMT) is a biological process in which epithelial cells lose their cell junctions and apicobasal polarity, undergo cytoskeletal reorganization, secrete extracellular matrix (ECM) components, and consequently transdifferentiate into migratory mesenchymal cells[1]. EMT is essential for proper embryonic development, as well as for tissue remodeling and wound healing. The abnormal reactivation of EMT plays a role in the progression of various human diseases, especially those linked to tissue fibrosis, cancer cell invasion, and metastasis[1–3]. EMT is mainly induced by the EMT transcription factors (EMT-TFs), including SNAI1, SLUG, TWIST1 and ZEB1/2, which repress the promoter activity of genes encoding epithelial markers, such as E-cadherin, and induce the expression of mesenchymal markers, including N-cadherin, Vimentin and Fibronectin[1,3]. The cytokine transforming growth factor-β (TGF-β) is a main driver of EMT in cancer[4–7].

TGF-β signaling is initiated upon TGF-β ligand binding to the cell surface complexes of type I and type II serine/threonine kinase receptors (TβRI and TβRII, respectively). TβRI recruits and phosphorylates regulated (R)-SMAD2/3, which form heteromeric complexes with SMAD4 that accumulate in the nucleus. Together with other transcription factors, the SMAD2/3/4 complex contacts to DNA and stimulates the transcription of target genes such as *PAI-1*, *CTGF* and EMT-TFs, including *SNAI1*[8,9]. TGF-β signaling is fine-tuned at multiple levels including the receptor level[10,11]. By recruiting the SMAD-Specific E3 Ubiquitin Protein Ligase 1/2 (SMURF1/2), the inhibitory protein SMAD7 binds and targets activated TβRI for polyubiquitination and degradation[12–14].

Long non-coding RNAs (lncRNAs) are transcripts exceeding 200 nucleotides in length and lack protein-coding potential[15]. LncRNAs can function as guides, scaffolds, and decoys to influence interactions between biological macromolecules, such as protein-protein and protein-DNA interactions, and thereby modulate gene expression at various levels[16,17]. In particular, enhancer RNAs (eRNAs), a subclass of

[1]Oncode Institute and Department of Cell and Chemical Biology, Leiden University Medical Center, Leiden, The Netherlands. [2]Oncode Institute, Hubrecht Institute-KNAW and University Medical Center Utrecht, Utrecht, The Netherlands. [3]Department of Biomedical Data Sciences, Sequencing Analysis Support Core, Leiden University Medical Center, Leiden, The Netherlands. [4]Department of Medical Biochemistry and Biophysics, SciLifeLab and Karolinska Institute, Solna, Sweden. [5]These authors contributed equally: Chuannan Fan, Qian Wang. ✉e-mail: q.wang@lumc.nl; p.ten_dijke@lumc.nl

nuclear lncRNAs transcribed from active enhancer loci, play a critical role in facilitating local enhancer activities and enhancer-promoter looping to influence gene transcription[18,19]. For example, *SCREEM* (*SNAI1 cis-regulatory eRNA expressed in monocytes*) eRNAs, produced from a *SNAI1* enhancer region, enhance *SNAI1* expression in a *cis*-regulatory manner, thereby promoting EMT in human primary bronchial epithelial cells[20]. Although several studies have implicated lncRNAs in the modulation of TGF-β signaling[21–23], the interplay between eRNAs and TGF-β signaling in EMT is not well-characterized.

In this work, we perform a CRISPR activation (CRISPRa)[24]-based screen in breast cancer cells and identify TGF-β-induced *SNAI1 enhancer RNA* (*SNAI1e*; *SCREEM2*) that strongly promotes TGF-β/SMAD signaling by attenuating TβRI degradation. Mechanistically, *SNAI1e* binds bromodomain containing protein 4 (BRD4) to enforce the local enhancer activity and stimulate *SNAI1* transcription. SNAI1 interacts with and retains SMAD7 in the nucleus, thereby antagonizing TβRI polyubiquitination and degradation. We characterize *SNAI1e* as an eRNA that promotes TGF-β signaling and EMT-associated hallmarks, including increased motility, invasion, stemness, and therapy resistance in cancer cells.

Results

TGF-β-induced *SNAI1e* is an enforcer of TGF-β signaling

We sought to identify key lncRNAs that potentiate TGF-β signaling in breast cancer cells. Toward this end, we conducted a functional screen on TGF-β-induced lncRNAs, as TGF-β-induced gene products frequently act as negative or positive feedback regulators of TGF-β signaling[23,25]. Reanalysis of our previous transcriptome data enriched 107 lncRNAs, whose expression was induced upon TGF-β stimulation at early (2 h), intermediate (8 h) and late (24 h) time points in MDA-MB-231 triple-negative breast cancer (TNBC) cells[21] (Supplementary Fig. 1a, Supplementary Table 1). We performed a CRISPRa-based gain-of-function screen in MDA-MB-231 cells that stably express a selective synthetic SMAD3/4-driven transcriptional reporter, $CAGA_{12}$-dynGFP[26], to monitor the TGF-β/SMAD-induced transcriptional output (Fig. 1a). For each lncRNA hit, we designed 5 gRNAs, which fell within 500 bp upstream and 200 bp downstream of the transcripts' annotated transcription start sites (TSSs)[27,28]. MDA-MB-231 cells were transduced with a gRNA library targeting 107 lncRNAs at a low multiplicity of infection (MOI) to obtain only one gRNA per cell. Upon TGF-β treatment for 48 h, cells were sorted into two groups (GFP-high and -low; Fig. 1a and "Methods" section) by fluorescence-activated cell sorting (FACS). Screen hits were ranked based on the comparison of gRNA distributions between the GFP-high and GFP-low populations in two biological replicates (Fig. 1b, Supplementary Data 1). gRNAs targeting positive control genes, i.e. two CAGA minimal promoter (MLP) regions, *TBRII* and *RNF11* (encoding an E3 ubiquitin ligase that targets inhibitory SMAD7), potentiated TGF-β/SMAD signaling, which validated the technical robustness (Fig. 1b). Of note, multiple lncRNAs enforced the TGF-β-induced transcriptional response with similar potency as the positive controls (Fig. 1b). We focused on one of the top hits, *SCREEM2*[20], and renamed it as *SNAI1 enhancer RNA* (*SNAI1e*) due to its proximity to *SNAI1* in the human genome (Supplementary Fig. 1b) and its regulatory role in *SNAI1* gene expression (as detailed below).

The 5′ and 3′ rapid amplification of cDNA ends (RACE) assays demonstrated that *SNAI1e* is a 4055 nt one-exon transcript nearly identical to the annotated lncRNA *lnc-SNAI1-5:2* in the LNCipedia database[29], or *NONHSAG110604.1* in the NONCODE database[30], differing only by the absence of a single adenine at the 5′ end (Supplementary Fig. 1c, d and Supplementary Table 2). Assessing the kinetic *SNAI1e* expression pattern upon TGF-β stimulation by RT-qPCR showed that TGF-β induced an early increase of *SNAI1e* expression, and that the induction was sustained until 72 h in MDA-MB-231 cells (Fig. 1c). Similar results were obtained in MCF10A-M2 pre-malignant breast and A549 non-small cell lung adenocarcinoma cells (Supplementary Fig. 1e, f). To verify *SNAI1e* as a target gene of TGF-β/SMAD signaling, we depleted *SMAD4* with a short hairpin (sh) RNA and found a dramatic suppression of both basal and TGF-β-induced *SNAI1e* expression in MDA-MB-231 cells (Fig. 1d, Supplementary Fig. 1g). Next, we characterized the *SNAI1e* promoter by cloning a 2640 bp DNA fragment (Promoter 1 (P1); −2472 to +168; chromosome 20: 50,027,744-50,030,383, GRCh38.p14) upstream the *SNAI1e* TSS and placed it at the 5′ end of a luciferase gene (Supplementary Fig. 1h). TGF-β treatment, along with the ectopic expression of SMAD3 or constitutively active (ca)TβRI, enhanced the reporter activity of *SNAI1e* P1 in HepG2 cells (Fig. 1e). Chromatin immunoprecipitation (ChIP)-qPCR demonstrated that RNA polymerase (Pol) II bound to the *SNAI1e* TSS (−99 - +53; chromosome 20: 50,030,117-50,030,268,GRCh38.p14) and the binding was facilitated by TGF-β stimulation in MDA-MB-231 cells (Fig. 1f). Analysis of the promoter truncation mutants revealed a minimal DNA fragment (P7; −2072 to -2026; chromosome 20: 50,028,143 to 50,028,190 (GRCh38.p14)) that was required for TGF-β/SMAD-triggered *SNAI1e* promoter activity (Fig. 1g, Supplementary Fig. 1h and i). Mutation of the putative SMAD3 binding element abrogated both basal and TGF-β-induced *SNAI1e* promoter activity, suggesting that activated SMAD3 directly contacts the *SNAI1e* promotor (Fig. 1g). ChIP-qPCR consolidated the direct binding of SMAD3 to the *SNAI1e* promoter, which was increased upon TGF-β treatment in MDA-MB-231 cells (Fig. 1h). Bioinformatic analysis with Coding Potential Assessment Tool (CPAT)[31] predicted a lack of coding potential of *SNAI1e* (Fig. 1i). Subcellular fractionation followed by RT-qPCR was performed to explore *SNAI1e* localization in MDA-MB-231 cells, as this information may aid in elucidating its mechanism of action. *SNAI1e* was mainly localized in the nucleus (Fig. 1j), which was further validated by fluorescence in situ hybridization (FISH) in MDA-MB-231 cells (Fig. 1k). TGF-β stimulation did not change *SNAI1e* cytoplasmic and nuclear distribution (Fig. 1k). Taken together, these results demonstrate that *SNAI1e* is a TGF-β/SMAD-induced nuclear lncRNA that promotes TGF-β/SMAD signaling.

SNAI1e promotes TGF-β-induced EMT and cancer cell migration

To evaluate the correlation between *SNAI1e* expression and breast cancer progression, we analyzed several TCGA datasets[32] and observed that *SNAI1e* expression was significantly higher in tumor samples from breast cancer patients in comparison to that of normal breast tissues (Fig. 2a). In line with this result, *SNAI1e* was more highly expressed in TNBC cell lines than in MCF10A-M1 normal breast cells, MCF10A-M2 pre-malignant breast cells, and the less aggressive MCF7 luminal breast cancer cells (Fig. 2b). To explore the effect of *SNAI1e* on EMT, we activated endogenous *SNAI1e* expression using two individual CRISPRa guide RNAs (gRNAs) in epithelial MCF10A-M2 and A549 cells (Supplementary Fig. 2a, b). CRISPRa-guided increased expression of *SNAI1e* potentiated TGF-β-induced downregulation of the expression of epithelial marker E-cadherin, and upregulation of the expression of mesenchymal markers, including N-cadherin, Fibronectin, Vimentin and SNAI1 (Fig. 2c, d). On the contrary, GapmeR-mediated *SNAI1e* knockdown mitigated the changes in EMT marker expression triggered by TGF-β in MCF10A-M2 cells (Fig. 2e and Supplementary Fig. 2c). In agreement with these results, *SNAI1e* overexpression augmented, but GapmeR-mediated *SNAI1e* knockdown attenuated, TGF-β-induced filamentous actin (F-actin) stress fiber formation in A549 cells (Fig. 2f, g, Supplementary Fig. 2d). Additionally, *SNAI1e* overexpression promoted, whereas *SNAI1e* depletion inhibited, TGF-β-induced cell migration in MDA-MB-231 cells (Fig. 2h, i, Supplementary Fig. 2e, f). To validate our in vitro findings, an in vivo zebrafish embryo breast cancer xenograft model[33] was applied, where *SNAI1e* promoted breast cancer cell extravasation (Fig. 2j, k). Moreover, to consolidate the results from GapmeR-directed loss-of-function experiments, an orthogonal approach CRISPR interference (CRISPRi)[34] was used to diminish *SNAI1e*

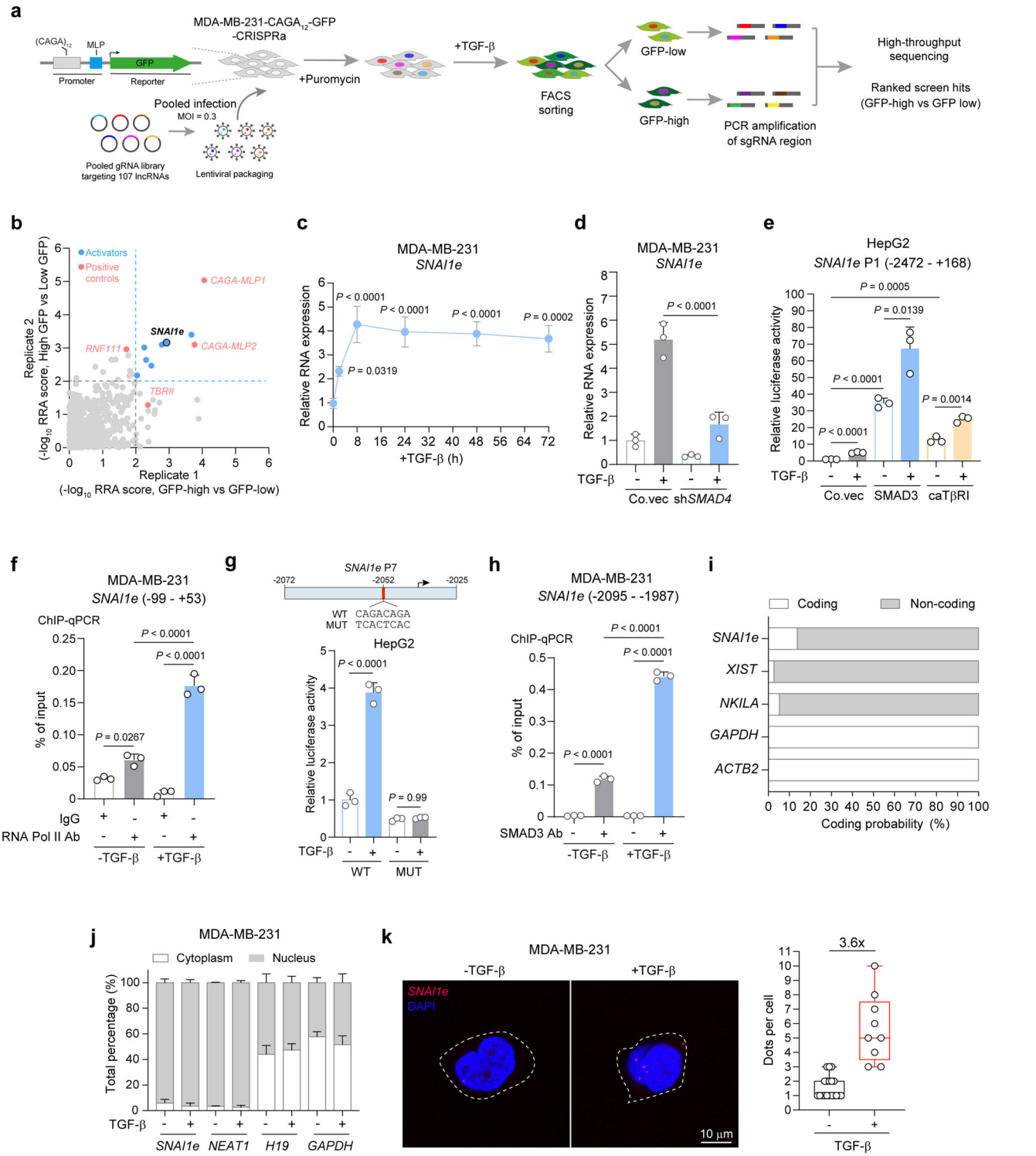

expression (Supplementary Fig. 2g–m). Since EMT is correlated with the gain of stemness and chemotherapy resistance in cancer cells[7,35,36], we assessed the mammosphere formation abilities of MCF10A-M2 cells upon *SNAI1e* overexpression. As expected, *SNAI1e* enhanced mammosphere formation in MCF10A-M2 cells (Fig. 2l), which was accompanied by an increase of $CD44^{+}CD24^{-}$ breast cancer stem cell population[37] (Supplementary Fig. 2n). Consistent with these observations, *SNAI1e* overexpression conferred greater resistance to the chemotherapeutic drugs Doxorubicin (Doxo) and Paclitaxel (PTX) in MCF10A-M2 cells (Fig. 2m, n). Collectively, our results reveal that TGF-β-induced *SNAI1e* strongly promotes TGF-β-induced EMT, migration, stemness and/or drug resistance in breast and lung cancer cells (Supplementary Fig. 2o).

SNAI1e inhibits TβRI polyubiquitination and degradation

Next, we validated the effects of *SNAI1e* on promoting TGF-β signaling. The dynamic activity of the $CAGA_{12}$-dynGFP reporter revealed that CRISPRa-mediated *SNAI1e* overexpression facilitated the TGF-β-induced transcriptional response in MDA-MB-231 cells (Fig. 3a). In contrast, *SNAI1e* knockdown by GapmeR, CRISPR/Cas13d[38] or CRISPRi reduced the TGF-β-induced reporter activity (Fig. 3b, Supplementary Fig. 3a–c). Consistently, transcriptome analysis enriched TGF-β target

Fig. 1 | TGF-β-induced *SNAI1e* is an enforcer of TGF-β signaling. a Schematic overview of CRISPRa-mediated lncRNA screen. **b** Diagram of lncRNA screening results. **c** RT-qPCR analysis of *SNAI1e* expression in MDA-MB-231 cells upon TGF-β stimulation. The results are presented as mean ± SD from three biological replicates. **d** RT-qPCR analysis of *SNAI1e* expression in MDA-MB-231 cells upon shRNA-mediated *SMAD4* knockdown. Co.sh, empty vector for shRNA expression. The results are expressed as the mean ± SD from three biological replicates. **e** Luciferase reporter assay to determine the effects of SMAD3 and caTβRI on *SNAI1e* promoter 1 (P1) activity. The data are plotted as mean ± SD from three biological replicates. Co.vec, empty vector control. **f** ChIP-qPCR analysis of the *SNAI1e* transcription start site (TSS) in MDA-MB-231 cells. The results are expressed as mean ± SD from three biological replicates. **g** Luciferase reporter assay to determine the effects of TGF-β on *SNAI1e* promoter 7 (P7) activity. The data are presented as mean ± SD from three biological replicates. **h** ChIP-qPCR analysis of the *SNAI1e* promoter region (-2095 - -1987) in MDA-MB-231 cells. The results are expressed as mean ± SD from three biological replicates. **i** Coding probability prediction of *SNAI1e* with the CPAT software. Protein-coding mRNAs (*GAPDH* and *ACTB2*) and well-annotated lncRNAs (*XIST* and *NKILA*) serve as positive and negative controls, respectively. **j** Subcellular localization analysis of *SNAI1e* in MDA-MB-231 cells by RT-qPCR. *NEAT1* serves as positive control for the nuclear fraction, whereas *H19* and *GAPDH* serve as positive controls for the cytoplasmic fraction. The data are presented as mean ± SEM from three biological replicates. **k** RNA fluorescence in situ hybridization was performed to evaluate *SNAI1e* subcellular localization in MDA-MB-231 cells. Representative images from two independent experiments are shown. Scale bar = 10 μm. The results are quantified as a box plot with min to max Whiskers from 19 (−TGF-β) and 9 (+TGF-β) technical replicates (cells) and the fold change is shown. The boundaries of the box indicate the 25th percentile and the 75th percentile, and the center indicates the median. Significance was calculated using two-tailed unpaired Student's *t*-test (**e**), and one-way ANOVA followed by Dunnett's (**c**) and Tukey's (**d**, **f**, **g**, **h**) multiple comparisons test. gEV gRNA expression vector. Co.vec empty control vector. Ab antibody.

genes, including *IL11*, *SNAI1*, *PMEPA1* and *ANGPTL4*, as top genes upregulated by *SNAI1e* in MDA-MB-231 cells (Fig. 3c). We conducted pathway enrichment analysis on the 84 *SNAI1e*-upregulated genes and identified TGF-β signaling and EMT as the most significantly impacted cellular processes by *SNAI1e* overexpression (Fig. 3d, Supplementary Fig. 3d). Moreover, gene set enrichment analysis (GSEA) confirmed a strong positive correlation between manipulated *SNAI1e* expression and the TGF-β response gene signature or the EMT gene signature (Fig. 3e, Supplementary Fig. 3e). However, no correlation was found between *SNAI1e* expression and the response gene signatures of BMP, WNT, and YAP (Supplementary Fig. 3f–h). In addition, *SNAI1e* overexpression promoted the expression of TGF-β target genes (i.e., *PAI-1*, *CTGF*, and *SMAD7*), and *SNAI1e* depletion showed the opposite effect in MDA-MB-231 cells (Supplementary Fig. 3i–k). Interestingly, *SNAI1e* overexpression facilitated TGF-β-induced SMAD2 phosphorylation (p-SMAD2) in MDA-MB-231 cells (Fig. 3f), while this effect was suppressed upon *SNAI1e* depletion (Fig. 3g, Supplementary Fig. 3l). This observation prompted us to investigate the impact of *SNAI1e* on TGF-β receptor expression, as p-SMAD2 is a direct indicator of TGF-β receptor activity. *SNAI1e* overexpression elevated TβRI, but not TβRII, protein expression in MDA-MB-231 cells (Fig. 3h), whereas CRISPRi-mediated *SNAI1e* knockdown suppressed TβRI protein expression (Supplementary Fig. 3m). However, *TBRI* and *TBRII* mRNA levels were not altered by *SNAI1e* in MDA-MB-231 cells (Supplementary Fig. 3n), suggesting that *SNAI1e* may modulate TβRI protein stability. Consistent with this notion, cycloheximide (CHX)-directed time-course experiments revealed that *SNAI1e* protected TβRI protein from degradation in MDA-MB-231 cells (Fig. 3i). To determine whether TβRI degradation involves the proteasome or lysosome, MDA-MB-231 cells with *SNAI1e* knockdown were challenged with proteasomal or lysosomal inhibitors. We found that the proteasomal inhibitor MG132, but not the lysosomal inhibitor Bafilomycin (BafA1), restored TβRI expression in *SNAI1e* depletion cells (Fig. 3j). In agreement with this result, *SNAI1e* elicited an inhibitory effect on TβRI polyubiquitination in MDA-MB-231 cells (Fig. 3k and Supplementary Fig. 3o). Blocking TβRI kinase activity with the selective small molecule inhibitor SB431542 (SB)[39] alleviated the changes of EMT marker expression and cell migration by CRISPRa-directed *SNAI1e* overexpression (Fig. 3l, m). On the contrary, TβRI ectopic expression counteracted the suppressive effect of *SNAI1e* knockdown on migration in MDA-MB-231 cells (Fig. 3n, o), suggesting that TβRI is a crucial target of *SNAI1e* in promoting EMT and migration.

SNAI1e selectively induces *SNAI1* expression

We sought to decipher the mechanism by which *SNAI1e* potentiates TβRI stability and TGF-β/SMAD signaling. SNAI1 has been implicated in reinforcing TGF-β/SMAD signaling in breast cancer cells[40,41]. Considering that *SNAI1e* is localized in the nucleus (Fig. 1k), and the close proximity between *SNAI1e* and *SNAI1* in the human genome (Supplementary Fig. 1b), we hypothesized that *SNAI1e* directly targets *SNAI1* for transcriptional activation to promote TGF-β/SMAD signaling. Both basal and TGF-β-induced *SNAI1* mRNA and protein levels were dramatically increased upon *SNAI1e* overexpression in MDA-MB-231 cells (Fig. 4a, b), supporting the RNA-seq results mentioned above (Fig. 3c). In contrast, *SNAI1e* depletion by multiple approaches (i.e. GapmeR, siRNA, Cad13d, and CRISPRi) greatly reduced *SNAI1* expression in MDA-MB-231 cells (Fig. 4c, d and Supplementary Fig. 4a–d). Importantly, the expression of the other neighboring genes was unaffected upon CRISPRa-mediated *SNAI1e* overexpression in MDA-MB-231 cells (Supplementary Figs. 1b, 4e).

GSEA showed a positive correlation between *SNAI1e* expression and *SNAI1*-induced gene signature, indicating that *SNAI1* is a key downstream effector of *SNAI1e* (Fig. 4e). To validate the effect of *SNAI1* on enhancing TGF-β/SMAD signaling, a Tet-ON inducible system was used for *SNAI1* ectopic expression. Doxycycline (Dox) treatment showed a dose-dependent induction of *SNAI1* expression in MDA-MB-231 cells (Supplementary Fig. 4f). We selected 0.1 μg/mL of Dox to stimulate *SNAI1* expression in the following experiments (Supplementary Fig. 4f), as this concentration induced ectopic *SNAI1* expression at levels comparable to those induced by *SNAI1e* in MDA-MB-231 cells (Fig. 4a). As expected, ectopic *SNAI1* expression promoted the TGF-β-induced transcriptional response and p-SMAD2, as well as TβRI protein expression in MDA-MB-231 cells (Fig. 4f, Supplementary Fig. 4g, h). Moreover, TβRI polyubiquitination was suppressed upon *SNAI1* overexpression in MDA-MB-231 cells (Fig. 4g). To further evaluate whether *SNAI1* is essential for *SNAI1e* to promote TGF-β/SMAD signaling, we used an shRNA to deplete *SNAI1* (Fig. 4h). We found that *SNAI1* knockdown diminished the increase of TGF-β-induced p-SMAD2 and downstream reporter activity upon *SNAI1e* overexpression in MDA-MB-231 cells (Fig. 4h and Supplementary Fig. 4i).

SNAI1 has been reported to enhance TβRI expression in MDA-MB-231 cells[40], but the underlying mechanism remains unclear. Since SMAD7 and SNAI1 are both localized in the nucleus, we assumed that SNAI1 may bind SMAD7. Indeed, we observed a SMAD7-SNAI1 interaction that was even stronger than the SMAD4-SNAI1 interaction, which served as a positive control[42], in HEK293T cells (Fig. 4i). Proximity ligation assays (PLA) confirmed the endogenous SNAI1-SMAD7 interaction in the nucleus of MDA-MB-231 cells (Fig. 4j). Next, we tested the effect of SNAI1 overexpression on SMAD7 localization. SNAI1 retained SMAD7 protein in the nucleus of MDA-MB-231 cells as shown by immunofluorescence staining (Fig. 4k) and subcellular fractionation followed by western blotting (Fig. 4l). Taken together, our data demonstrate that *SNAI1e* induces *SNAI1* expression at the transcriptional level, and SNAI1 protein binds and sequesters SMAD7 protein in the nucleus to decrease TβRI polyubiquitination and proteasomal degradation (Fig. 4m).

https://doi.org/10.1038/s41467-025-58032-w

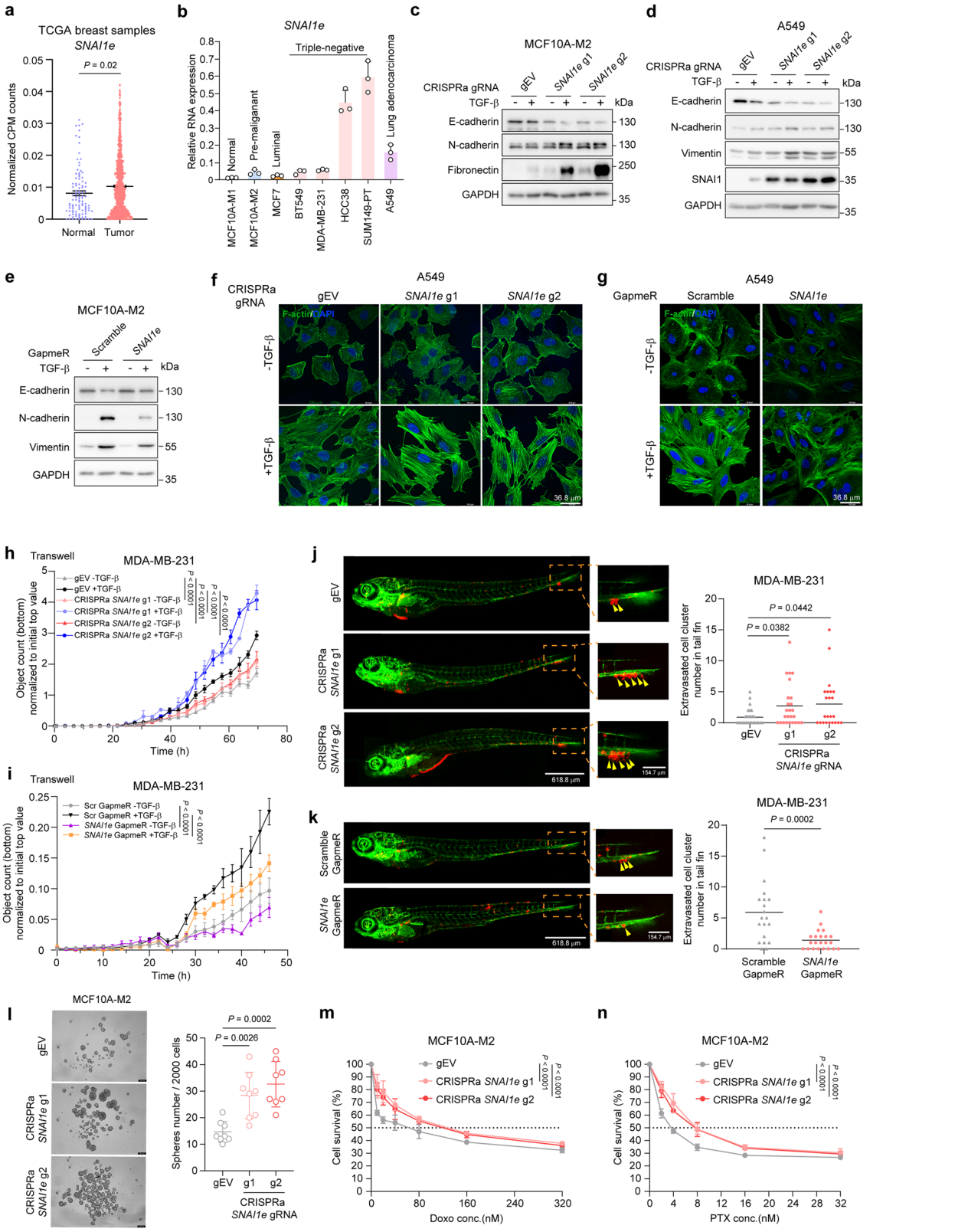

***SNAI1e* functions as an eRNA to facilitate *SNAI1* transcription**

Given the proximity of *SNAI1e* gene body to *SNAI1* in the human genome (Supplementary Fig. 1b), we hypothesized that *SNAI1e* transcribes from an enhancer region and functions as an eRNA[18,19] to activate *SNAI1* transcription. Firstly, we performed Circular Chromosome Conformation Capture (4C)-seq[43] to analyze the chromatin interactions between *SNAI1e* gene body, which was used as a bait (viewpoint; VP), and its surrounding DNA regions in MDA-MB-231 cells (Fig. 5a). We observed that the highest peak, representing the most potent *SNAI1e* interaction site, was in the genomic region of *SNAI1* (Fig. 5a). Interestingly, TGF-β stimulation facilitated the *SNAI1e*-*SNAI1* genomic interaction (Fig. 5a). Next, we quantified the abundance of two specific histone modifications associated with active enhancers (i.e. H3 lysine 27 acetylation (H3K27ac) and H3 lysine 4 monomethylation

Fig. 2 | *SNAI1e* promotes TGF-β-induced EMT and migration. a Comparison of *SNAI1e* expression between normal and tumor breast samples from the TCGA dataset. The results are expressed as mean ± SEM from 101 normal and 1002 tumor breast samples, respectively. **b** RT-qPCR analysis of *SNAI1e* expression in multiple cell lines. The data are plotted as mean ± SD from three biological replicates. **c**–**e** Effect of *SNAI1e* on TGF-β-induced EMT marker expression in MCF10A-M2 (**c**, **e**) or A549 (**d**) cells upon CRISPRa-mediated *SNAI1e* overexpression (**c**, **d**) or GapmeR-mediated *SNAI1e* knockdown (**e**). **f**, **g** Immunofluorescence analysis of F-actin expression in A549 cells upon CRISPRa-mediated *SNAI1e* overexpression (**f**) or GapmeR-mediated *SNAI1e* knockdown (**g**). Scale bar = 36.8 µm. **h**, **i** Transwell assay to evaluate the effect of *SNAI1e* on TGF-β-induced migration in MDA-MB-231 cells. *SNAI1e* overexpression and knockdown were achieved by CRISPRa (**h**) and GapmeR (**i**), respectively. The results are expressed as mean ± SD from eight (**h**) and four (**i**) biological replicates, respectively. **j**, **k** In vivo zebrafish xenograft experiments with MDA-MB-231 cells upon CRISPRa-mediated *SNAI1e* overexpression (**j**) or GapmeR-mediated *SNAI1e* knockdown (**k**). Extravasated breast cancer cell clusters are indicated with yellow arrows. Whole zebrafish image, bar = 618.8 µm; zoomed image, bar = 154.7 µm. The results are expressed as mean from 27 (gEV), 25 (g1), and 23 (g2) biological replicates in (**j**), and from 20 (Scramble GapmeR) and 22 (*SNAI1e* GapmeR) biological replicates in (**k**), respectively. **l** Effect of CRISPRa-mediated *SNAI1e* overexpression on mammosphere formation in MCF10A-M2 cells. The numbers of mammospheres are presented as mean ± SD from eight biological replicates. Scale bar = 100 µm. **m**, **n** Dose-response curves for doxorubicin (Doxo; **m**) or paclitaxel (PTX; **n**) in MCF10A-M2 cells upon CRISPRa-mediated *SNAI1e* overexpression The results are expressed as mean ± SD from three biological replicates. Significance was assessed using two-tailed unpaired Student's *t*-test (**a**, **k**), two-way ANOVA followed by Dunnett's (**h**, **i**) and Tukey's (**m**, **n**) multiple comparisons test, and one-way ANOVA followed by Dunnett's multiple comparisons test (**j**, **l**). Data are representative of two (**f**, **g**) and at least three (**c**–**e**) independent experiments with similar results. gEV gRNA expression vector. Scr scramble.

(H3K4me1))[44–46] by performing ChIP-qPCR with multiple primer pairs targeting the *SNAI1e* gene body region (Fig. 5b). We found that these two histone markers were enriched in the *SNAI1e* gene body region, with their abundance further increased by TGF-β treatment in MDA-MB-231 cells (Fig. 5c). Next, we employed CRISPR/Cas9 with paired gRNAs to deplete the *SNAI1e* gene body in MDA-MB-231 cells (Supplementary Fig. 5a). As expected, *SNAI1* expression was reduced in two independent knockout (KO) clones compared to wild-type (WT) MDA-MB-231 cells (Supplementary Fig. 5b, c). These results suggest that the gene body region of *SNAI1e* functions as an enhancer that targets *SNAI1* in the human genome.

To investigate the role of *SNAI1e* as an eRNA in targeting *SNAI1* for transcriptional activation, we checked the recruitment of RNA Pol II and the trimethylation of histone H3 lysine 4 (H3K4me3), a marker of transcription initiation[47,48], at the *SNAI1* TSS (−38 to +83, chromosome 20 49,982,942–49,983,062, GRCh38.p14). As expected, ChIP-qPCR results showed that CRISPRa-mediated *SNAI1e* overexpression promoted the enrichment of both RNA Pol II and H3K4me3 at the TSS of *SNAI1* in MDA-MB-231 cells (Fig. 5d). To eliminate the potential confounding effect of CRISPRa on altering local enhancer activity, and to separately assess the role of *SNAI1e* from that of the enhancer itself, we depleted *SNAI1e* using GapmeR. *SNAI1e* knockdown inhibited RNA Pol II recruitment at the *SNAI1* TSS (Fig. 5e). To further confirm this result, we employed the CRISPR-Display system[49] to tether *SNAI1e* to the *SNAI1e* gene body. *SNAI1e* was directed to two genomic loci of the *SNAI1e* gene body using two independent gRNAs and the deactivated Cas9 (dCas9; Supplementary Fig. 6a, b). A short variant, *SNAI1e-variant1* (*SNAI1e-V1*; *lnc-SNAI1-5:1*), derived from the same enhancer region, was included for analysis (Supplementary Fig. 6a). In this setup, *in cis* overexpression of *SNAI1e* (but not *SNAI1e-V1*) using two gRNAs promoted *SNAI1* expression (Fig. 5f, Supplementary Fig. 6c). Consistent with its role as an eRNA functioning *in cis*, ectopic *SNAI1e* expression (uncoupled from gRNAs) did not affect *SNAI1* expression (Fig. 5f, Supplementary Fig. 6c). Consistently, ectopic *SNAI1e* expression using a lentiviral vector did not affect *SNAI1* expression or TGF-β/SMAD signaling (Supplementary Fig. 7a–e). Taken together, these results suggest that TGF-β-induced *SNAI1e* stimulates its local enhancer activity, marked by increased H3K27ac and H3K4me1 levels, and thereby triggers *SNAI1* transcription by promoting the recruitment of RNA Pol II and H3K4me3 to the *SNAI1* TSS (Fig. 5g).

SNAI1e directly binds to BRD4

BRD4 interacts with acetylated histones and eRNAs at enhancer regions through its bromodomains (BDs) to stimulate local enhancer activities and facilitate transcriptional elongation[50,51]. We speculated that *SNAI1e* may bind BRD4 to alter the local chromatin landscape for enhancer activation. RNA immunoprecipitation (RIP)-qPCR demonstrated that *SNAI1e* co-immunoprecipitated with BRD4, but not with the negative control nuclear protein YTH N6-methyladenosine RNA-binding protein C1 (YTHDC1), from MDA-MB-231 cell lysates (Fig. 6a). Consistently, biotinylated *SNAI1e*, but not its antisense counterpart (*SNAI1e-AS*) or the negative control nuclear lncRNA *LETS1*[22], pulled down ectopically expressed BRD4 protein in HEK293T cells (Fig. 6b). To map the binding region of BRD4 on *SNAI1e*, we divided *SNAI1e* into 4 fragments (T1–T4), each representing a quarter of the *SNAI1e* sequence (Supplementary Fig. 8). RNA pull-down analysis demonstrated that only the 5′ fragment (T1; 1–1023) was able to interact with BRD4, although its binding capacity was dampened compared to the full-length *SNAI1e* (Fig. 6c). Furthermore, we investigated the BRD4 domain(s) responsible for *SNAI1e* binding by analyzing BRD4 truncation mutants (Fig. 6d). Depletion of either of the two bromodomains (BD1 or BD2) abolished the interaction between BRD4 and *SNAI1e*, indicating that the tandem bromodomains are essential for BRD4 binding to *SNAI1e* (Fig. 6e). In vitro RIP-qPCR was performed to assess the direct interaction between BRD4-BD1/2 and *SNAI1e*. Compared to the mock control and the negative control recombinant FLAG-tagged SMURF2 protein, recombinant FLAG-BRD4-BD1/2 exhibited direct binding to *SNAI1e* (Fig. 6f). Consistent with this finding, in vitro RNA pull-down further validated the direct association between BRD4-BD1/2 and *SNAI1e* (Fig. 6g).

BRD4 is required for *SNAI1e* to induce *SNAI1* expression and EMT

Since eRNAs have been implicated in facilitating BRD4 binding to local enhancer regions[50], we checked whether BRD4 binds to the *SNAI1e* gene body, and if any such interaction would be impacted by *SNAI1e*. Given that BRD4 binds to highly acetylated chromatin[51,52], we selected two H3K27ac-enriched regions (Region 2 and Region 9) within the *SNAI1e* gene body, as identified in Fig. 5c. ChIP-qPCR results demonstrated that *SNAI1e* depletion by GapmeR or CRISPRi suppressed BRD4 association with the two *SNAI1e* gene body regions in MDA-MB-231 cells (Fig. 7a, Supplementary Fig. 9a). On the contrary, CRISPR-Display-mediated *in cis* tethering of *SNAI1e* transcript (but not *SNAI1e-V1* transcript) by two gRNAs enhanced BRD4 recruitment to the two *SNAI1e* gene body regions, respectively (Fig. 7b). To investigate whether *BRD4* is required for *SNAI1e* to elicit its biological effects, we utilized two independent shRNAs to knockdown *BRD4* in MDA-MB-231 cells (Fig. 7c). We observed that *SNAI1e*-induced *SNAI1* mRNA expression was reduced upon *BRD4* knockdown in MDA-MB-231 cells (Fig. 7d). In addition, masking of histone acetyl-lysine-binding pockets in BRD4 with the small molecule inhibitor JQ-1[53] confirmed the role of BRD4 in promoting *SNAI1* expression upon both CRISPRa- and CRISPR-Display-mediated *SNAI1e in cis* overexpression (Fig. 7e, f, Supplementary Fig. 9b). Moreover, under both TGF-β-stimulated and unstimulated conditions, JQ-1 treatment reduced *SNAI1e*-induced migration in MDA-MB-231 (Fig. 7g) and decreased *SNAI1e*-induced changes in EMT marker expression in MCF10A-M2 cells (Fig. 7h). Additionally, JQ-1 suppressed *SNAI1e*-induced in vivo extravasation of MDA-MB-231 cells in zebrafish embryos (Fig. 7i) and reduced mammosphere formation

https://doi.org/10.1038/s41467-025-58032-w

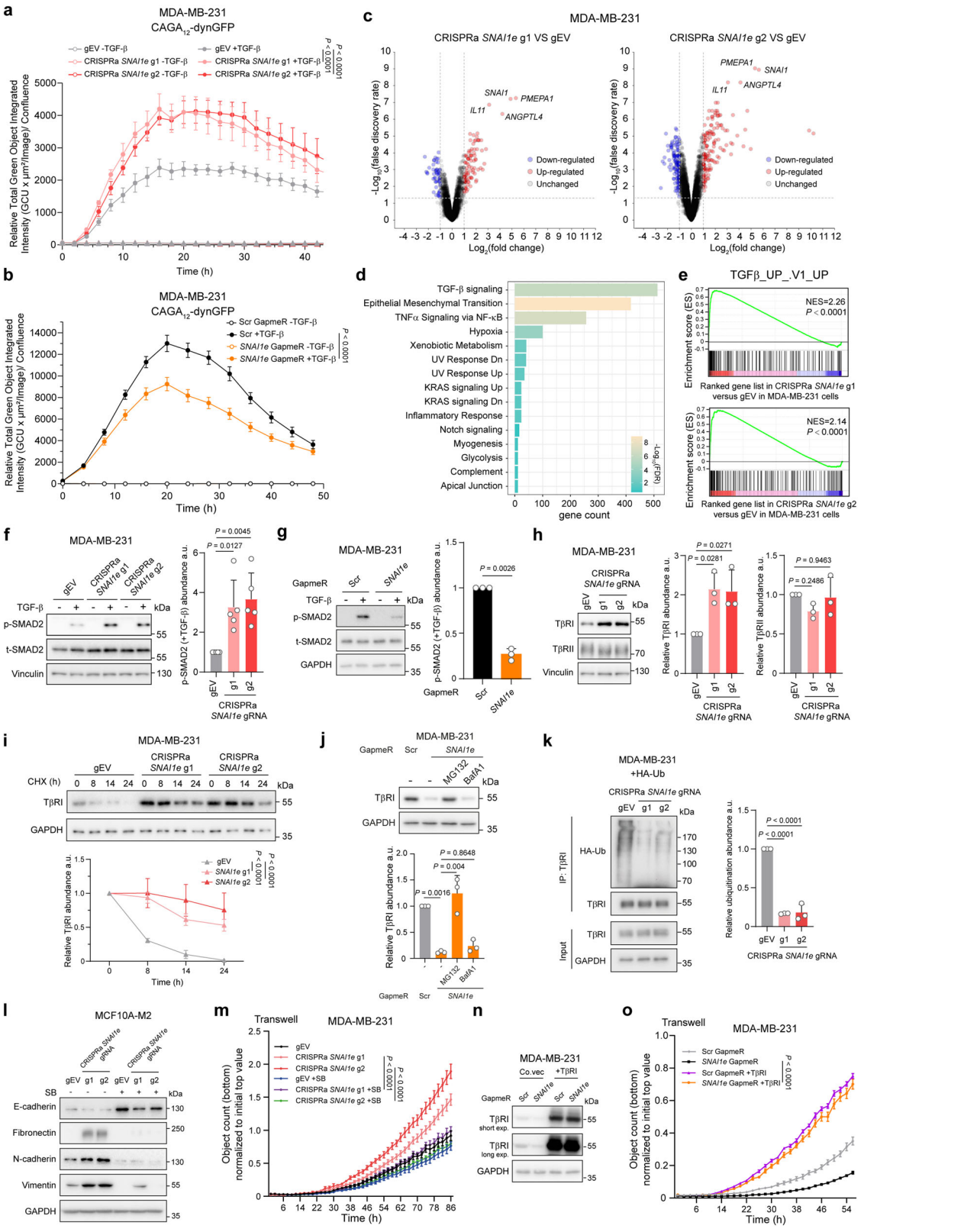

by MCF10A-M2 cells (Fig. 7j). Taken together, our results suggest that blocking BRD4 with JQ-1 inhibits *SNAI1e*-induced *SNAI1* expression, EMT, and migration in breast cancer cells (Fig. 7k).

Discussion

Our study proposes a mechanism by which a *cis*-regulatory eRNA potentiates TGF-β signaling. TGF-β induces *SNAI1e* expression from a *SNAI1* enhancer region. *SNAI1e* interacts with and facilitates BRD4 enrichment on the local enhancer, resulting in the promotion of the enhancer activity and upregulation of *SNAI1* expression. SNAI1 interacts with and sequesters SMAD7 in the nucleus, leading to the suppression of TβRI polyubiquitination and degradation. As a consequence, TGF-β signaling, TGF-β-induced EMT and migration are strengthened by *SNAI1e* in breast cancer cells. We demonstrated that

Fig. 3 | *SNAI1e* inhibits TβRI polyubiquitination and degradation. a, **b** Effect of *SNAI1e* overexpression (**a**) and knockdown (**b**) on $CAGA_{12}$-dynGFP reporter in MDA-MB-231 cells. The data are presented as mean ± SD from four (**a**) and twelve (**b**) biological replicates. **c** Volcano plots showing the differentially expressed genes upon *SNAI1e* overexpression. **d** Plot exhibiting the top 15 cellular processes affected by *SNAI1e*. **e** GSEA of correlations between *SNAI1e* and the TGF-β response gene signature. **f**, **g** Effect of *SNAI1e* overexpression (**f**) and knockdown (**g**) on TGF-β-induced p-SMAD2. The relative abundance of p-SMAD2 is shown as mean ± SD from five (**f**) and three (**g**) independent experiments. **h** Effect of *SNAI1e* overexpression on TβRI and TβRII protein expression. The relative abundance of TβRI and TβRII is shown as mean ± SD from three independent experiments. **i** Western blotting analysis of TβRI protein stability upon *SNAI1e* overexpression. Quantitative data show the relative TβRI abundance as mean ± SEM from four independent experiments. **j** Western blotting analysis of TβRI expression upon *SNAI1e* knockdown with the lysosome or proteasome inhibitors. Quantitative data show the relative TβRI abundance as mean ± SD from three independent experiments. **k** Effect of *SNAI1e* overexpression on TβRI polyubiquitination. Relative ubiquitination abundance is shown as mean ± SD from three independent experiments. **l** Effect of SB431542 (SB) on TGF-β-induced EMT marker expression in MCF10A-M2 cells upon *SNAI1e* overexpression. **m** Effect of SB431542 (SB) on MDA-MB-231 cell migration upon *SNAI1e* overexpression. The results are expressed as mean ± SEM from six biological replicates. **n** Western blotting results showing TβRI ectopic expression upon *SNAI1e* knockdown. **o** Effect of TβRI ectopic expression on MDA-MB-231 cell migration upon *SNAI1e* knockdown. The results are expressed as mean ± SEM from six biological replicates. Significance was assessed using non-parametric permutation test (**e**), two-tailed paired Student's *t*-test (**g**), two-way ANOVA followed by Tukey's (**a**, **m**, **o**) and Dunnett's (**b**, **i**) multiple comparisons test, and one-way ANOVA followed by Tukey's (**j**) and Dunnett's (**f**, **h**, **k**) multiple comparisons test. Data are representative of at least three (**l**, **n**) independent experiments with similar results. gEV gRNA expression vector. Scr scramble. Co.vec empty control vector. a.u. arbitrary units.

SNAI1e was more highly expressed in TNBC cell lines compared to normal breast cells and less-malignant cancer breast cell lines. The differences in basal *SNAI1e* expression across these four TNCB cell lines may be attributed to intrinsic genetic mutations or epigenetic changes, which require further investigation.

SNAI1 expression is tightly controlled at multiple levels, from epigenetic modifications to post-translational regulation[54]. In response to TGF-β, SMAD3 directly binds to the *SNAI1* promoter to stimulate transcriptional activation[55,56]. Moreover, SNAI1 can interact with SMAD3/4 and form a transcriptional repressor complex[42]. We discovered that *SNAI1e* is a direct target gene of TGF-β/SMAD signaling, and that *SNAI1e* depletion greatly mitigated TGF-β-induced *SNAI1* expression, suggesting that TGF-β induces *SNAI1e* to promote *SNAI1* expression in a feedforward loop. These results add another layer of regulation to TGF-β-induced *SNAI1* expression. A recent study demonstrates that RAS-responsive element-binding protein 1 (RREB1) binds to and primes *SNAI1* enhancer regions for TGF-β-induced activation, which is required for transcriptional activation of *SNAI1* by TGF-β in mouse lung adenocarcinoma cells[57]. This aligns with our findings that TGF-β induces the enrichment of H3K27ac and H3K4me1 at the *SNAI1e* gene body region in MDA-MB-231 cells. Further investigation is needed to determine whether *SNAI1e* interacts with RREB1 to enhance *SNAI1* enhancer activity. In addition to serving as a TGF-β/SMAD signaling effector to drive EMT[42], SNAI1 has been reported to reinforce TGF-β/SMAD signaling by enhancing TβRI protein expression in breast cancer cells[40]. Our results support this notion and further elucidated that SNAI1 interacts with and sequesters SMAD7 in the nucleus to alleviate TβRI polyubiquitination and proteasomal degradation. However, we have not excluded the possibility that SMAD7 binding may affect the transcriptional repressor activity of SNAI1.

We characterized *SNAI1e* gene body as an active enhancer and validated a direct and specific contact between the gene bodies of *SNAI1e* and *SNAI1* by 4C-seq analysis. As a subclass of nuclear lncRNAs transcribed from enhancer regions, eRNAs contribute to alterations in their local enhancer landscape[58,59]. We showed that *SNAI1* expression was downregulated upon CRISPR/Cas9-mediated knockout of the entire enhancer region, but this method cannot separate the specific role of *SNAI1e* from that of the enhancer itself. To address this issue, we employed two complementary methods, GapmeR and CRISPR-Display, which specifically target the *SNAI1e* transcript for manipulation while preserving the integrity of the enhancer. Results from CRISPR-Display confirmed that *SNAI1e* induces *SNAI1* expression in an *in cis* manner, highlighting the function of *SNAI1e* as a *cis*-regulatory eRNA. Moreover, these approaches excluded the potential effects of CRISPRa and CRISPRi on enhancer activity. A recent study identified the *SCREEM* locus as an enhancer region that induces *SNAI1* expression, and thereby promotes EMT in human primary bronchial epithelial cells and regulates monocyte differentiation[20]. The authors demonstrated that *SNAI1e*, also referred to as *SCREEM2*, is one of three eRNAs (*SCREEM1-3*) produced from this locus[20]. A strong positive correlation between the expression of *SNAI1e* and *SNAI1* was observed in monocytes[20], supporting our findings that *SNAI1* is one of the most upregulated genes upon *SNAI1e* overexpression in breast cancer cells. However, the previous study was unable to discriminate whether *SNAI1* activation was driven by the *SCREEM* locus itself or by its transcripts[20]. The authors suggested that *SCREEM* transcripts might be indispensable or function redundantly, as shRNA-mediated depletion of individual *SCREEM* eRNAs did not reduce *SNAI1* expression[20]. In contrast, our study employed GapmeR, which outperforms shRNA or siRNA for nuclear transcript knockdown[60], to deplete *SNAI1e* and observed a significant reduction in *SNAI1* expression across all the tested cell lines. Moreover, we confirmed this result using the orthogonal method of Cas13d-mediated depletion of the *SNAI1e* transcript. Furthermore, our CRISPR-Display results suggest that, despite being part of an eRNA cluster, *in cis* overexpression of *SNAI1e* alone is sufficient to activate *SNAI1* expression. However, eRNAs generally exhibit a tissue-specific expression pattern and therefore play a role in activating their neighboring target gene expression in confined types of tissues[19,61,62]. Further investigation is needed to determine whether the effects of *SNAI1e* on promoting *SNAI1* expression and TGF-β signaling can be expanded to other disease models.

We uncovered that locally transcribed *SNAI1e* maintains enhancer activity by interacting with BRD4. BRD4 has been shown to promote GLI family zinc finger 1 (Gli1)-induced *SNAI1* transcription in breast cancer cells[63] and to prevent SNAI1 protein degradation by competing with the E3 ligases FBXL14 and β-TRCP1 in gastric cancer cells[64]. Our findings provide further insight into BRD4-mediated multi-level regulation of SNAI1 expression. Moreover, we found that *SNAI1e* binds to BRD4 through direct interaction with its two BD domains to reinforce BRD4 association with the histone modification H3K27ac. This is consistent with a previous study in which BRD4 tandem BD domains were found to be required for interaction with a broad spectrum of eRNAs in colon cancer cells[50]. BD domains are known to recognize histone acetyl-lysine residues in promoters and enhancers[65]. It is likely that the BD region binding to *SNAI1e* is distinct from the one recognizing histone acetyl-lysine. This is supported by previous studies indicating that BD point mutations disrupt DNA binding without altering acetyl-lysine association affinity[66,67]. Hence, *SNAI1e* binding may change the BRD4 conformation toward a state for enhanced interactions with acetyl-lysines. However, given that BD domains are essential for BRD4 binding to both acetylated histones and *SNAI1e*, a comparison between full-length BRD4 and a BRD4 BD domain truncation mutant cannot clearly discriminate the effects of BRD4-*SNAI1e* interaction from those of BRD4-histone interaction in our study.

We demonstrated that the 1000 nt fragment at the 5′ end of *SNAI1e* (*SNAI1e*-T1) is required for *SNAI1e* to bind BRD4. However, BRD4

https://doi.org/10.1038/s41467-025-58032-w

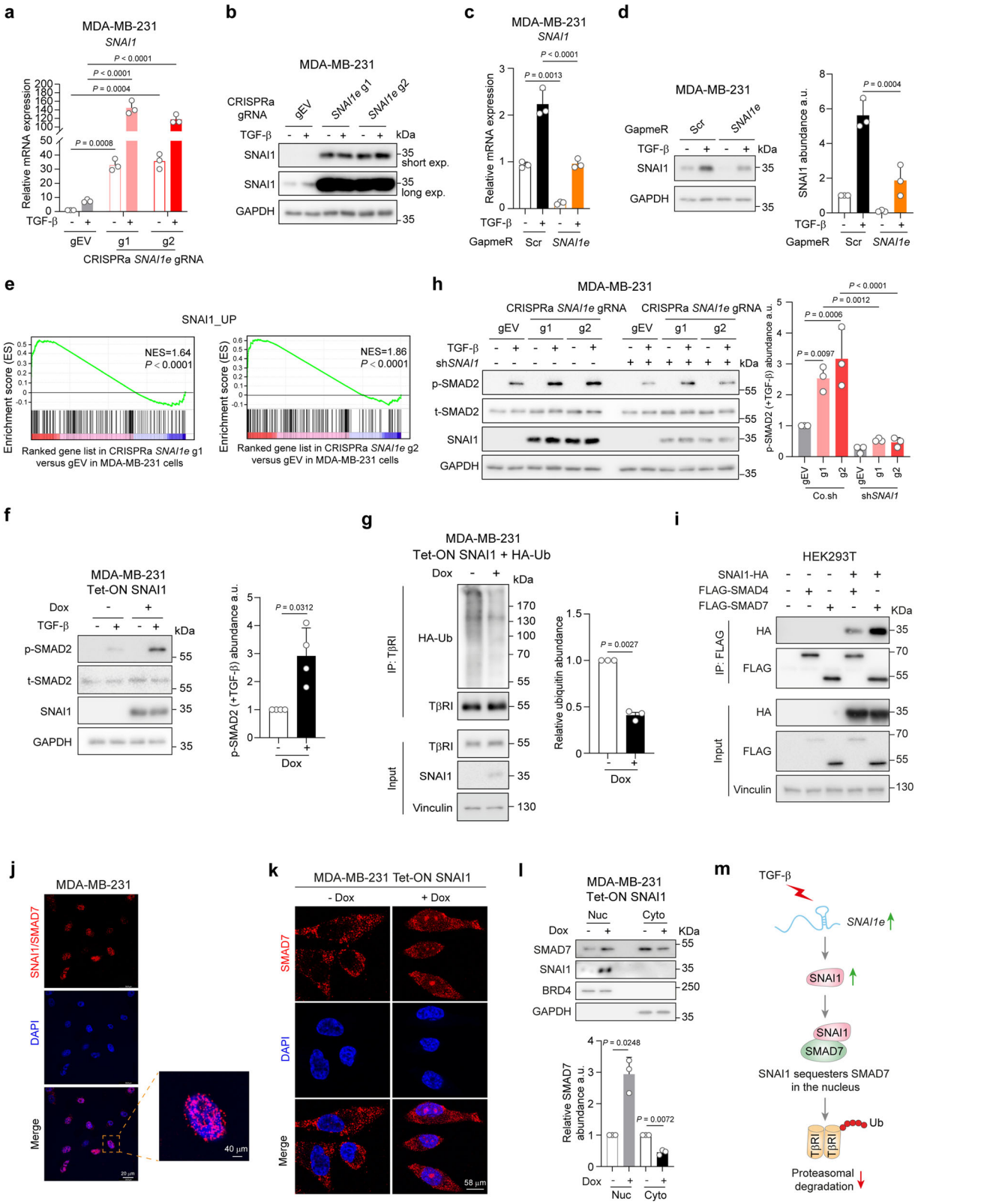

could not interact as potently with *SNAI1e*-T1 as full-length *SNAI1e*. Given that the folding structure of lncRNAs determines their interactions with proteins[68,69], it is possible that *SNAI1e* truncation may dampen its original folding structure that is needed for BRD4 binding. Further investigation may focus on mapping the minimal BRD4 binding region on *SNAI1e* by other approaches such as cross-linking and immunoprecipitation (CLIP) coupled with RNA footprinting[70] in live cells. Our ChIP-qPCR results, conducted upon CRISPR-Display-directed *SNAI1e in cis* tethering, demonstrated that *SNAI1e* can facilitate BRD4 enrichment at the local enhancer. However, we cannot exclude the possibility that this effect may result from the alteration of H3K27ac at the local enhancer due to changes in the overall level of gene transcription. To further discriminate the *SNAI1e*-dependent BRD4 recruitment from acetylated histone-mediated BRD4 enrichment,

Fig. 4 | *SNAI1e* induces *SNAI1* expression. a RT-qPCR analysis of *SNAI1* expression in MDA-MB-231 cells upon *SNAI1e* overexpression. The results are expressed as the mean ± SD from three biological replicates. **b** Effect of *SNAI1e* overexpression on SNAI1 protein expression. **c** RT-qPCR analysis of *SNAI1* expression upon *SNAI1e* knockdown. The data are presented as mean ± SD from three biological replicates. **d** Effect of *SNAI1e* knockdown on SNAI1 protein expression. Quantitative data show the relative abundance of SNAI1 as mean ± SD from three independent experiments. **e** GSEA of correlations between *SNAI1e* expression and *SNAI1*-induced gene signature. NES, normalized enrichment score. **f** Effect of SNAI1 ectopic expression on TGF-β-induced p-SMAD2 in MDA-MB-231 cells. Quantitative data show the abundance of p-SMAD2 as mean ± SD from three independent experiments. **g** Effect of SNAI1 ectopic expression on TβRI polyubiquitination in MDA-MB-231 cells expressing HA-ubiquitin (HA-Ub). Relative ubiquitination is shown as mean ± SEM from three independent experiments. **h** Effect of *SNAI1e* overexpression and shRNA-mediated *SNAI1* knockdown on TGF-β-induced p-SMAD2. Quantitative data show the abundance of p-SMAD2 as mean ± SD from three independent experiments. **i** Interactions between SNAI1 and SMAD4 or SMAD7 were analyzed by co-immunoprecipitation assays in HEK293T cells. **j** The endogenous SNAI1-SMAD7 interaction as evaluated by PLA. The red and blue dots indicate the SNAI1-SMAD7 interaction and the staining of nuclei by DAPI, respectively. Scale bar = 20 µm (left image) and 40 µm (right image). **k** Immunofluorescence analysis of SMAD7 localization upon SNAI1 ectopic expression. Scale bar = 58 µm. **l** Western blotting analysis of SMAD7 localization upon SNAI1 ectopic expression. The levels of the cytoplasmic marker GAPDH and the nuclear marker BRD4 serve as positive controls. Relative SMAD7 abundance is shown as mean ± SD from three independent experiments. **m** Schematic working model. *SNAI1e*-induced SNAI1 interacts with and potentiates SMAD7 nuclear retention, resulting in the decrease of TβRI polyubiquitination and proteasomal degradation. Significance was assessed using two-way ANOVA followed by Šidák's multiple comparisons test (**a**), one-way ANOVA followed by Tukey's multiple comparisons test (**c**, **d**, **h**), non-parametric permutation test (**e**), and two-tailed paired Student's *t*-test (**f**, **g**, **l**). Data are representative of at least three (**b**, **i**–**k**) independent experiments with similar results. gEV gRNA expression vector. Scr scramble. a.u. arbitrary units. Nuc nucleus. Cyto cytoplasm.

future studies could focus on disrupting the minimal core region required for BRD4 binding in *SNAI1e*, while preserving its structural integrity. This could be achieved using advanced RNA editing systems[71,72]. Besides functioning as a scaffold protein, BRD4 acetylates histone H3 at Lys122 (H3K122) through its intrinsic histone acetyltransferase domain[73]. Whether *SNAI1e* binding affects BRD4-histone modification activities warrants further investigation.

Our findings underscore a significant role of BRD4 in *SNAI1e*-driven EMT, migration, and stemness, as demonstrated by both BRD4 genetic and pharmacological inhibition. Given that BRD4 is widely expressed across tissues and is critical in normal physiological processes, such as hematopoiesis and host immune response[74,75], systemic targeting BRD4 with selective inhibitors can cause undesirable on-target effects, including digestive system dysfunctions and metabolic disorders in (pre) clinical trials[52,76], which greatly limit the therapeutic application of BRD4 inhibitors in cancer treatment. Moreover, cancer cells gain resistance to BRD4 inhibition after prolonged treatment in preclinical studies[77,78]. Since EMT inhibition can suppress both cancer cell invasion and drug resistance[2], targeting *SNAI1e* to suppress EMT in cancer cells may overcome the toxicity and drug resistance associated with BRD4 inhibitors.

Methods

Lentiviral CRISPRa screen

MDA-MB-231-CAGA$_{12}$-GFP cells were created by lentiviral, single-copy integration of CAGA$_{12}$-GFP and isolating a single cell clone that showed good induction in response to TGF-β. pLenti-dCas9-VP64-BFP (Addgene; 196711) was packaged into lentivirus in HEK293T (ATCC) using plasmids psPAX2 (Addgene; 12260, a gift from Dr. D. Trono, Swiss Federal Technology Institute of Lausanne, Lausanne, Switzerland) and pCMV-VSV-G (Addgene; 8454, a gift from Dr. R.A. Weinberg, Whitehead Institute for Biomedical Research, Cambridge, MA, USA). The virus-containing supernatant was concentrated 40-fold with Lenti-X concentrator (Takara), aliquoted and stored in liquid nitrogen. MDA-MB-231-CAGA$_{12}$-GFP cells were then transduced with pLenti-dCas9-VP64-BFP, and a stable BFP positive population was isolated by repeated cell sorting (Sony SH800). gRNA sequences were designed against the 694 CAGE peaks from the FANTOM5 (GRCh38 v9 DPI clustering) dataset[27,28] which fell within 500 bp upstream and 200 bp downstream of the transcripts' annotated start sites, using a −300 to 0 window relative to the maximum of the CAGE peak. CRISPick[79,80] was used to design and rank gRNAs, and the top five ranked gRNAs were included in the library. 400 non-targeting control gRNAs as well as positive control gRNAs against known TGF-β-pathway genes and the promoter region of the CAGA$_{12}$-MLP were also included. The guide library was synthesized (Genscript), including an anchor sequence enabling synthesis of several libraries on the same array[80], double stranded using an ultramer containing random sequence labels[81] and amplified with primers CRISPRa_fw and CRISPRa_rev. The anchor sequence was removed by digestion with EcoRV, and the resulting final insert was cloned by Gibson assembly into pXPR_502 digested with BsmBI/EcoRI (Addgene; 96923, a gift from Dr. J.G. Doench and Dr. D. Root, Broad Institute of MIT and Harvard, Cambridge, MA, USA). The library plasmid was sequenced by NGS to confirm gRNA representation and packaged into lentivirus as described above. The functional titer of the library virus was estimated from the fraction of surviving cells after transduction with serial dilutions of virus followed by puromycin selection. dCas9-VP64 expressing MDA-MB-231-CAGA$_{12}$-GFP cells were then transduced with the library virus in duplicate at an approximate MOI of 0.3 and a coverage of 1000 cells per gRNA in the presence of 2 µg/ml polybrene. Transduced cells were selected with 2 µg/ml puromycin. A control sample was harvested on day 5 post transduction (p.t., early time point). Cell numbers per replicate were kept at 1000× coverage throughout. On day 7 p.t., cells were treated with TGF-β (5 µg/ml) for 48 h. An unsorted control sample was harvested, and cells were sorted based on GFP expression, collecting the top and bottom 10% GFP. Genomic DNA was isolated using the QIAamp DNA Blood Mini (Qiagen), and gRNA and RSL sequences were amplified by PCR as described[81], but with modified primers PCR2_fw and PCR3_fw. The amplicon was sequenced (Illumina) reading 20 cycles Read 1 with custom primer CRISPRSeq; 10 cycles index read i7 to read the RSL (not used in data analysis), and six cycles index read i5 for the sample barcode. NGS data was analyzed with the MaGeCK software, v.0.5.6[82]. The data is presented in Fig. 1a. *x* and *y* axes represent the $-\log_{10}$ transformation of the positive robust ranking aggregation (RRA) scores comparing the GFP-high population to the GFP-low population. The dashed line indicates the cutoff of $-\log_{10}$ (RRA score) at 2. The primers used for library construction and NGS sequencing are listed in Supplementary Table 3.

Cell culture and reagents

HEK293T (CRL-1573), HepG2 (HB-8065), A549 (CRM-CCL-185), MDA-MB-231 (CRM-HTB-26), MDA-MB-436 (HTB-130), HCC38 (CRL-2314), BT549 (HTB-122), and MCF7 (HTB-22) cells were purchased from the American Type Culture Collection (ATCC). SUM149-PT is a gift from Dr. S.E. Le Dévédec (Leiden Academic Centre for Drug Research, Leiden, The Netherlands). The cells mentioned above were cultured in Dulbecco's modified Eagle medium (DMEM; Thermo Fisher Scientific; 41965062) supplemented with 10% fetal bovine serum (FBS; Thermo Fisher Scientific; 16000044) and 100 U/mL penicillin/streptomycin (Thermo Fisher Scientific; 15140163). MCF10A-M1 and MCF10A-M2 cells were kindly provided by Dr. F. Miller (Barbara Ann Karmanos Cancer Institute, Detroit, USA) and cultured in DMEM/F12 (GlutaMAX™ Supplement; Thermo Fisher Scientific; 31331028) containing 5% horse serum (Thermo Fisher Scientific; 26050088), 0.1 µg/mL cholera toxin

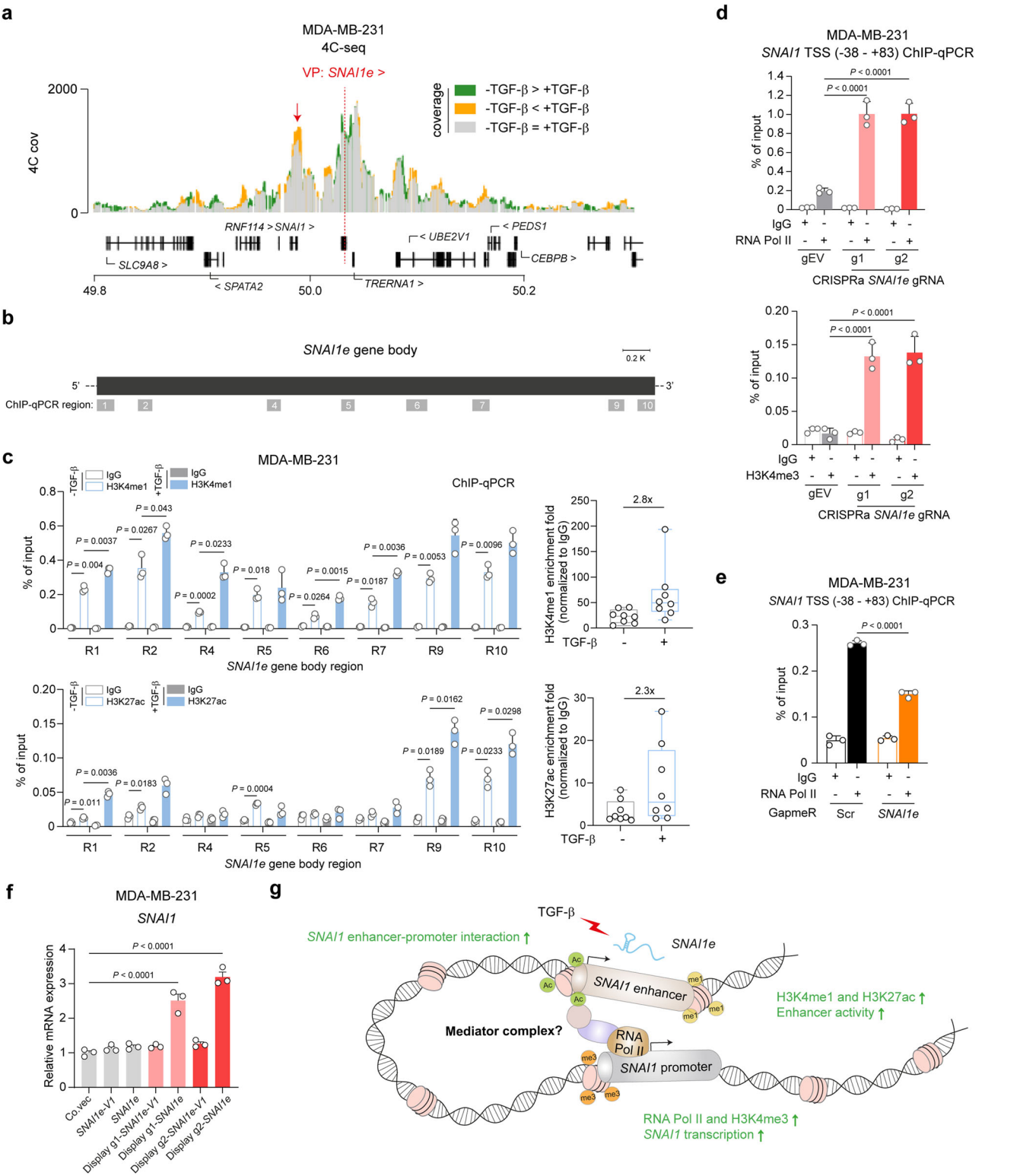

(Sigma–Aldrich; C8052), 0.02 μg/mL Epidermal Growth Factor (EGF; Sigma–Aldrich; 01-107), 0.5 μg/mL hydrocortisone (Sigma–Aldrich; H0135), 10 μg/mL insulin (Sigma–Aldrich; I6634) and 100 U/mL penicillin/streptomycin. All cell lines were maintained in a 5% CO_2, 37 °C humidified incubator, tested monthly for mycoplasma contamination and checked for authenticity by short tandem repeat (STR) profiling. Recombinant TGF-β3 is a kind gift from Dr. A. Hinck (University of Pittsburgh, Pittsburgh, USA). CHX (50 μg/mL; Sigma–Aldrich; C1988), BafA1 (5 μM for 6 h; Sigma–Aldrich; B1793) and MG132 (20 nM for 6 h; Sigma–Aldrich; 474787), Doxorubicin (Sigma–Aldrich; D5220), Paclitaxel (Sigma–Aldrich; T7191), SB431542 (1 μM) and JQ-1 (1 μM for 24 h; MedChemExpress; HY-13030) were used in the cell culture experiments.

Plasmid construction

Full-length *SNAIIe* was amplified by PCR from MDA-MB-231 cell-derived cDNA and inserted into the lentiviral vector pCDH-EF1α-MCS-polyA-PURO. The inducible vector for SNAI1 ectopic expression was generated

Fig. 5 | *SNAI1e* functions as an eRNA to facilitate *SNAI1* transcription. a Circular chromosome conformation capture (4C)-seq profile overlays displaying the *in cis* chromatin contacts of the *SNAI1e* gene body. The increased interactions between *SNAI1e* viewpoint (VP) and other regions in −TGF-β group or +TGF-β group are labeled in green or yellow, respectively. Common interactions are labeled in gray. Coverage represents an average of three biological replicates. y axis, 4C coverage per 1 million normalized reads. **b** Schematic of the amplified regions by the indicated primer pairs against the *SNAI1e* gene body. **c** ChIP-qPCR analysis of the H3K4me1 and H3K27ac enrichment within the *SNAI1e* gene body region in MDA-MB-231 cells. The data are shown as mean ± SD from three biological replicates. Cumulative analysis of the histone marker enrichment fold is shown as a box plot with min to max Whiskers from eight technical replicates (eight genomic regions). The boundaries of the box indicate the 25th percentile and the 75th percentile, and the center indicates the median. **d** ChIP-qPCR analysis of RNA Pol II and H3K4me3 enrichment at the *SNAI1* TSS upon CRISPRa-mediated *SNAI1e* overexpression. RT-qPCR results are shown as mean ± SD from three biological replicates. **e** ChIP-qPCR analysis of RNA Pol II enrichment at the *SNAI1* TSS upon GapmeR-mediated *SNAI1e* depletion. RT-qPCR results are shown as mean ± SD from three biological replicates. **f** RT-qPCR analysis of *SNAI1* expression in MDA-MB-231 cells upon CRISPR-Display-mediated *in cis* overexpression of *SNAI1e* or *SNAI1e-V1*. The data are presented as the mean ± SD from three biological replicates. **g** Schematic working model. TGF-β-induced *SNAI1e* stimulates local enhancer activity, marked by increased H3K27ac and H3K4me1 levels, and thereby triggers *SNAI1* transcription by promoting recruitment of RNA Pol II and H3K4me3 to *SNAI1* TSS. Significance was assessed by using two-way ANOVA followed by Dunnett's (**c**, **d**) Šídák's (**e**) multiple comparisons test, and one-way ANOVA followed by Tukey's multiple comparisons test (**f**). gEV gRNA expression vector. Co.vec control empty vector. Scr scramble. TSS transcription start site.

using Gateway cloning into the pLIX-403 vector (Addgene; 41395). BRD4 truncation mutants were amplified by PCR from pcDNA5-Flag-BRD4-WT (Addgene; 90331) and inserted into the pCDNA3.1-FLAG vector. CRISPRa, CRISPRi, and Cas13d gRNAs were inserted into the lentiviral vectors lenti sgRNA(MS2)_puro optimized backbone (Addgene; 73797), pLKO.1-U6-PURO-AA19 (kindly provided by Dr. M.A.F.V. Gonçalves, LUMC, Leiden, The Netherlands), and pHR_hU6-crScaffold_EF1a-PURO (modified from pSLQ5465_pHR_hU6-crScaffold_EF1a-PuroR-T2A-BFP; Addgene; 155307), respectively. CRISPR-Display gRNAs were cloned to a modified pCDNA.3.1 vector with a gRNA scaffold, followed by the insertion of *SNAI1e* or *SNAI1e-V1*. *SNAI1e* promoter fragments were amplified from MDA-MB-231 genomic DNA and subcloned into the pGL4-luc backbone (Promega). All plasmids were verified by Sanger sequencing, and the primers used for plasmid construction are listed in Supplementary Data 2.

Lentiviral transduction

Packaging plasmids (VSV, gag, and Rev) and expression constructs were cotransfected into HEK293T cells. At 48 h post-transfection, supernatants were collected and added to target cells. After 48 h of infection, selection antibiotics were added to the medium to ensure the selection of stable cells. We used shRNA constructs from Sigma–Aldrich for gene knockdown: TRCN0000040031 for *SMAD4* knockdown, TRCN0000199427 (#1) and TRCN0000318771 (#2) for *BRD4* knockdown, and TRCN0000063819 for *SNAI1* knockdown. lenti-dCAS-VP64_Blast (Addgene; 61425) and lenti-MS2-P65-HSF1_Hygro (Addgene; 61426) were used for the generation of CRISPRa stable cells. pHR-SFFV-dCas9-BFP-KRAB (Addgene; 46911) and pXR001: EF1a-CasRx-2A-EGFP (Addgene; 109049) were used for the generation of CRISPRi and CRISPR/Cas13d stable cells, respectively.

siRNA and GapmeR transfection

A final concentration of 25 nM scramble GapmeR (UGGGCGUAUA-GACGUGUUACAC) or GapmeR targeting *SNAI1e* (UGCAUCUGGA-CAGGGGUCUU) was transfected using lipofectamine 3000 (Thermo Fisher Scientific; L3000015). A final concentration of 25 nM non-targeting siRNA (siNT, Horizon) or siRNA targeting *SNAI1e* (UGCAU-CUGGACAGGGGUCUU, Horizon) was also transfected using lipofectamine 3000.

RT–qPCR

To detect TGF-β target gene (*PAI-1* and *CTGF*) and *SNAI1* expression, cells were treated with TGF-β (1 ng/ml) or vehicle control for 8 h. To check TGF-β–induced *SNAI1e* expression, TGF-β (5 ng/ml) or vehicle was added for indicated time points or 8 h, if the treatment duration is not specified. MDA-MB-231 cells with a Tet-ON system were treated with different doses of Doxycycline (Dox; 0.1 μg/mL) for 2 days to induce *SNAI1* expression. A NucleoSpin RNA kit (Macherey Nagel; 740955) was used to isolate total RNA from cells. Reverse transcription was carried out with a RevertAid RT Reverse Transcription Kit (Thermo Fisher Scientific; K1691). The indicated genes were amplified using the synthesized cDNA with specific primer pairs, and signals were visualized with a CFX Connect Real-Time PCR Detection System (Bio-Rad). *GAPDH* was used as the reference gene for normalization by the $2^{-\Delta\Delta Ct}$ method. The primer sequences used for RT–qPCR are listed in Supplementary Data 3. All experiments were performed at least three times, and representative results are shown.

Western blotting

To detect EMT marker expression, A549 or MCF10A-M2 cells were treated with TGF-β (1 ng/ml for A549 and 2.5 ng/ml for MCF10A-M2, respectively) or vehicle control for 1 day (A549) or 3 days (MCF10A-M2). To test JQ-1 effect on EMT marker expression, MCF10A cells were pre-treated without or with JQ-1 (1 μM) for 24 h before seeding. To check TGF-β–induced p-SMAD2, TGF-β (1 ng/ml) or vehicle control was added for indicated time points or 1 h, if the treatment duration is not specified. To check TGF-β–induced SNAI1 expression, TGF-β (5 ng/ml) or vehicle control was used to treat cells for 8 h. MDA-MB-231 cells with a Tet-ON system were treated with Doxycycline (Dox; 0.1 μg/mL) for 2 days to include SNAI1 expression. RIPA buffer (150 mM sodium chloride, 1.0% Triton-X-100, 0.5% sodium deoxycholate, 0.1% sodium dodecyl sulfate (SDS), and 50 mM Tris–HCl (pH 8.0)) supplemented with complete protease inhibitor cocktail (Roche; 11836153001) was applied to lyse cells. Subsequently, protein concentrations were evaluated with a DC™ protein assay kit (Bio-Rad; 5000111). Next, SDS–polyacrylamide gel electrophoresis (PAGE) was performed, and proteins were then transferred onto a 0.45-μm polyvinylidene difluoride (PVDF) membrane (Merck Millipore; IPVH00010). Subsequently, the membrane was blocked with 5% nonfat dry milk in Tris-buffered saline (TBS) with 0.1% Tween 20 detergent (TBST) for 1 h at room temperature. After probing the membranes with the corresponding primary and secondary antibodies, images were acquired with a ChemiDoc Imaging System (Bio-Rad). The primary antibodies are listed in Supplementary Table 4. All experiments were performed at least three times, and representative results are shown. ImageJ (National Institutes of Health, United States) was used to quantify relative protein expression levels by densitometry.

Chromatin immunoprecipitation (ChIP) assays

MDA-MB-231 cells were treated without or with TGF-β (5 ng/mL) for 24 h. 1×10^7 MDA-MB-231 cells were collected, cross-linked with 1% formaldehyde and sonicated into 200–700 bp fragments using sonication beads (Diagenode; C01020031). The collected supernatant was diluted five times and incubated with 5 μg of IgG (Cell Signaling Technology; 2729 and 5415), anti-RNA polymerase II antibody (Active Motif; 39097), anti-SMAD3 antibody (Abcam; ab208182), anti-H3K4me1 antibody (Active Motif; 39635), anti-H3K27ac antibody (Active Motif; 39685), anti-H3K4me3 antibody (Active Motif; 61379), or anti-BRD4 antibody (Cell Signaling Technology; 13440) overnight at 4 °C. The next day, the antibody-chromatin complex was captured by

30 μL of Protein A/G Sepharose beads. After five washes, followed by RNase A (Thermo Fisher Scientific; R1253) and Proteinase K (Thermo Fisher Scientific; 25530049) treatment, the DNA was extracted by isopropanol. RT-qPCR was performed to quantify the enrichment of protein at the regions of interest. Representative results from three independent experiments are shown.

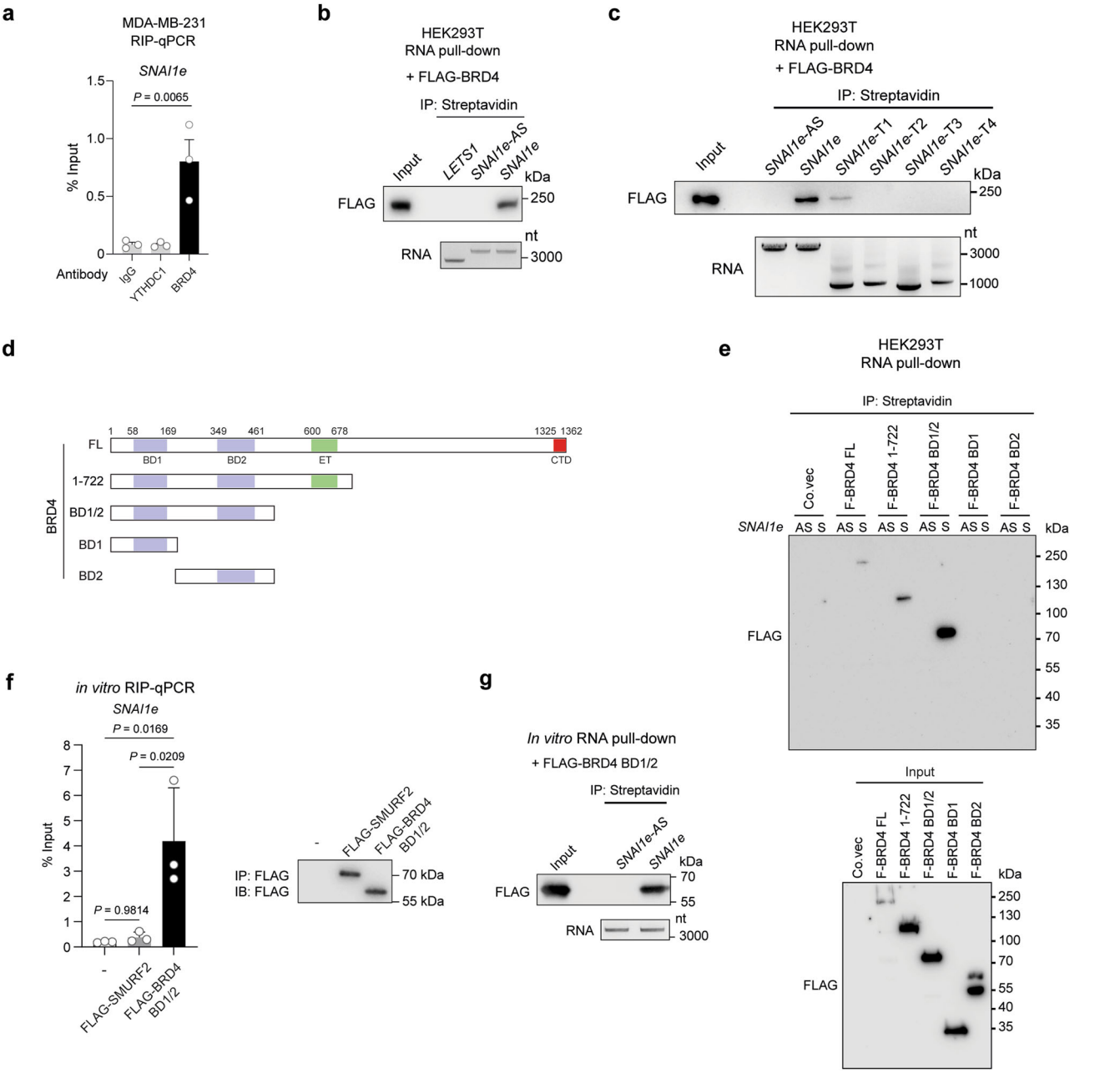

Fig. 6 | *SNAI1e* directly interacts with BRD4. a The interaction between *SNAI1e* and BRD4 in MDA-MB-231 cells was analyzed by RNA immunoprecipitation (RIP). YTHDC1 served as a negative control. RT-qPCR was performed to detect *SNAI1e* expression in immunoprecipitants from MDA-MB-231 cells. The results are expressed as mean ± SD from three independent experiments. **b** The interaction between *SNAI1e* and BRD4 in MDA-MB-231 cells was analyzed by RNA pull-down. Western blotting analysis was performed to detect FLAG expression in whole-cell lysates (Input) and immunoprecipitants (IP). *LETS1* and *SNAI1e-AS* served as negative controls. The RNA amounts used for pull-down were evaluated by agarose gel electrophoresis. **c** The interaction between *SNAI1e* truncation mutants and BRD4 in MDA-MB-231 cells was analyzed by RNA pull-down. Western blotting analysis was performed to detect FLAG expression in whole-cell lysates (Input) and immunoprecipitants (IP). The RNA amounts used for pull-down were evaluated by agarose gel electrophoresis. **d** Schematic representation of full-length (FL) BRD4 and the truncation mutants tested. **e** The interactions between *SNAI1e* and BRD4 FL or the truncation mutants in MDA-MB-231 cells were analyzed by RNA pull-down. *SNAI1e-AS*, antisense *SNAI1e*; *SNAI1e-S*, sense *SNAI1e*. Western blotting analysis was performed to detect FLAG expression in whole-cell lysates (Input) and immunoprecipitants (IP). The RNA amounts used for pull-down were evaluated by agarose gel electrophoresis. **f** The direct interaction between *SNAI1e* and the FLAG-BRD4 BD1/2 recombinant protein was analyzed by in vitro RIP. The results are expressed as mean ± SD from three independent experiments. The FLAG-tagged proteins in immunoprecipitants were evaluated by western blotting. **g** The direct interaction between *SNAI1e* and the recombinant FLAG-BRD4 BD1/2 protein was analyzed by in vitro RNA pull-down. Western blotting analysis was performed to detect FLAG expression in whole-cell lysates (Input) and immunoprecipitants (IP). The RNA amounts used for pull-down were evaluated by agarose gel electrophoresis. Significance was calculated by using one-way ANOVA followed by Dunnett's (**a**) and Tukey's (**f**) multiple comparisons test. Data are representative of at least three (**b**, **c**, **e**, **g**) independent experiments with similar results. Co.vec empty control vector.

https://doi.org/10.1038/s41467-025-58032-w

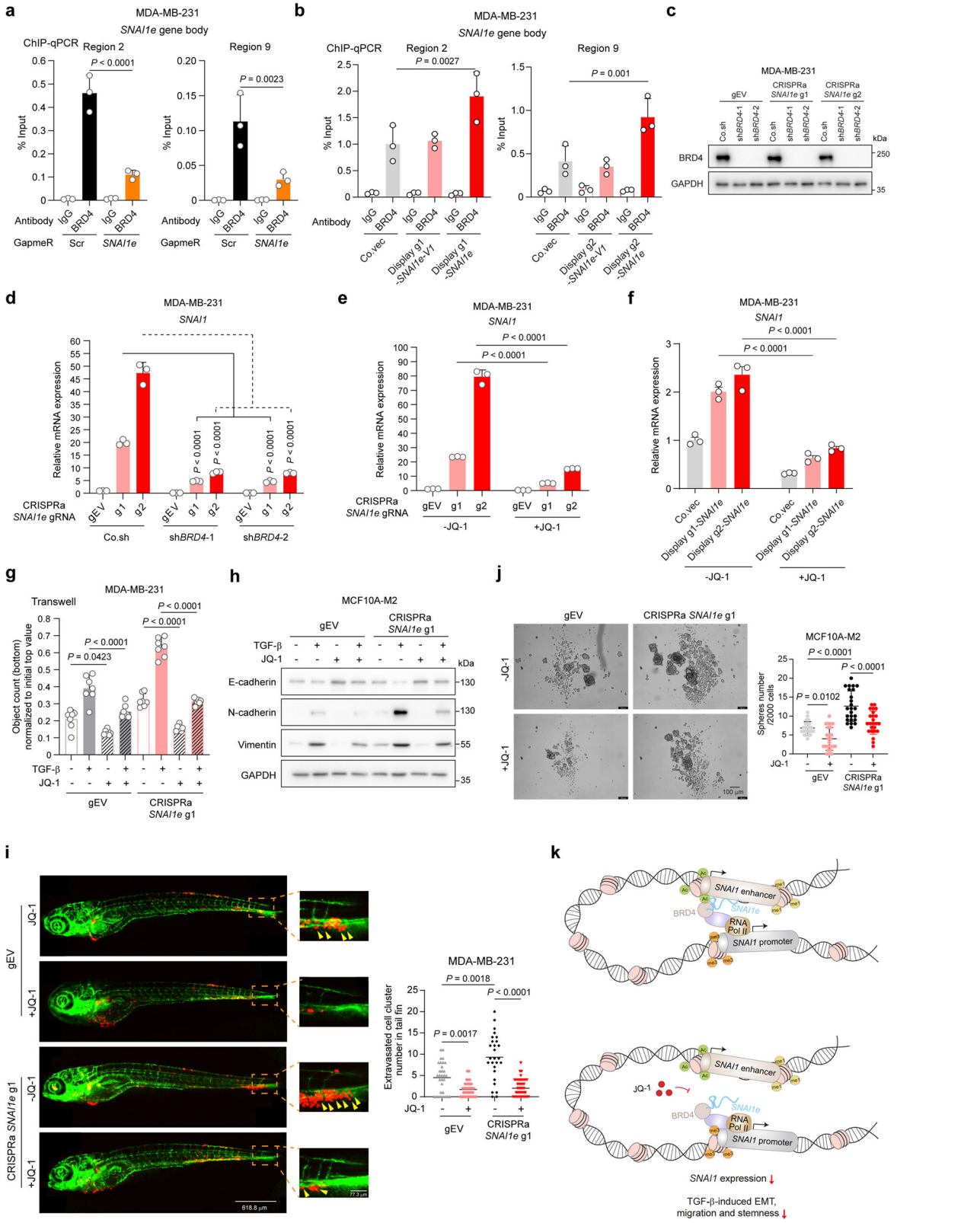

Race

RACE was performed on MDA-MB-231 cells using a 5′/3′ RACE Kit, 2nd generation (Roche; 03353621001). The resulting 5′/3′ RACE products were cloned to a pU.CAG.MSC2.rBGpA vector (kindly provided by Dr. M.A.F.V. Gonçalves, LUMC, Leiden, The Netherlands) and transformed into competent cells. Representative Sanger sequencing results from three independent colonies are presented.

CRISPR-Display

MDA-MB-231 cells were transfected with indicated constructs expressing gRNA fused to *SNAI1e* or *SNAI1e-V1*, along with a dCas9 expression construct (kindly provided by Dr. M.A.F.V. Gonçalves, LUMC, Leiden, The Netherlands), using Lipofectamine 3000 (Thermo Fisher Scientific; L3000015). 6 h post-transfection, medium was replaced with fresh DMEM medium containing JQ-1 (1 μM) or a vehicle control

Fig. 7 | BRD4 is required for *SNAI1e* to induce *SNAI1* expression and promote EMT and migration. a, **b** ChIP-qPCR analysis of BRD4 enrichment at two regions in *SNAI1e* gene body upon GapmeR-mediated *SNAI1e* knockdown (**a**) and CRISPR-Display-mediated *in cis* overexpression of *SNAI1e* or *SNAI1e-V1* (**b**). RT-qPCR results are shown as mean ± SD from three biological replicates. **c** Validation of the knockdown efficiency of *BRD4* by western blotting. **d** RT-qPCR analysis of *SNAI1e*-induced *SNAI1* expression upon *BRD4* knockdown. The results are shown as mean ± SD from three biological replicates. **e**, **f** Effect of JQ-1 on *SNAI1* expression induced by *SNAI1e* overexpression using CRISPRa (**e**) and CRISPR-Display (**f**). RT-qPCR results are shown as mean ± SD (**e**) and mean ± SEM (**f**) from three biological replicates. **g** A transwell migration assay was performed to evaluate the effect of JQ-1 on TGF-β/*SNAI1e*-induced migration in MDA-MB-231 cells. The results are expressed as mean ± SD from seven biological replicates. **h** Effect of JQ-1 on TGF-β/*SNAI1e*-induced EMT marker expression in MCF10A-M2 cells. **i** In vivo zebrafish extravasation experiments with MDA-MB-231 cells upon CRISPRa-mediated *SNAI1e* overexpression and JQ-1 treatment. Extravasated breast cancer cell clusters are indicated with yellow arrows. Whole zebrafish image, bar = 618.8 µm; zoomed image, bar = 77.3 µm. The results are expressed as mean from 31 (gEV-JQ-1), 36 (gEV +JQ-1), 27 (g1-JQ-1), and 41 (g1+JQ-1) biological replicates. **j** Mammosphere formation assays to check effect of JQ-1 and CRISPRa-mediated *SNAI1e* overexpression on MCF10A-M2 cell stemness. The numbers of mammospheres are expressed as mean ± SD from 24 biological replicates in the right panel. Scale bar = 100 µm. **k** Schematic working model. *SNAI1e* interacts with BRD4 to facilitate its binding to H3K27ac on the local enhancer, and thereby triggers *SNAI1* transcription, TGF-β-induced EMT, migration, and stemness. JQ-1 treatment disrupts BRD4 binding to the local enhancer and inhibits *SNAI1* transcription, TGF-β-induced EMT, migration, and stemness. Significance was assessed using one-way ANOVA followed by Dunnett's (**a**, **b**, **i**) and Tukey's (**d**–**g**, **j**) multiple comparisons test. Data are representative of at least three (**c**, **h**) independent experiments with similar results. gEV gRNA expression vector. Co.vec empty control vector. Scr scramble.

(DMSO). RNA and DNA samples were collected after 48 h post-transfection. ChIP-qPCR and RT-qPCR were performed as described above. All experiments were performed at least three times, and representative results are shown.

SNAI1e KO

MDA-MB-231 cells stably expressing Cas9 (Addgene; 98290) were transduced with gRNA expression constructs by lentivirus infection. Following puromycin selection, single cells were seeded into 96-well plates using a dilution method. Genomic DNA was isolated from multiple single clones using the Phire Tissue Direct PCR Master Mix kit (Thermo Fisher Scientific; F170L). The *SNAI1e* gene body region was characterized by PCR-based genotyping with LongAmp® Taq DNA Polymerase (NEB; M0323S). Two single clones exhibiting *SNAI1e* gene body depletion (*SNAI1e* KO) were selected for RT-qPCR analysis. A pool of MDA-MB-231-Cas9 cells transduced with an empty gRNA expression vector served as the control (WT).

Transcriptional reporter assays

Cells transfected with indicated constructs were serum-starved for 6 h and stimulated with TGF-β (5 ng/ml) or vehicle control for 16 h. Luciferase activity was measured with the substrate D-luciferin (Promega) and a luminometer (PerkinElmer) and normalized to β-galactosidase activity. MDA-MB-231 cell with stable expression of the $CAGA_{12}$-dynGFP reporter[26] was used to monitor the TGF-β-induced transcriptional response in an IncuCyte live cell imaging system (Essen BioScience). Cells were serum-starved for 16 h and stimulated without or with TGF-β (0.5 ng/mL). GFP intensity was quantified as total green integrated intensity normalized with cell confluence. All experiments were performed three times, and representative results are shown.

Immunofluorescent staining

To evaluate the expression and localization of SMAD7, MDA-MB-231 cells with a Tet-ON system for SNAI1 ectopic expression were treated without or with Doxycycline (Dox; 0.1 µg/mL) for 2 days. Cells were washed with phosphate-buffered saline (PBS), fixed, permeabilized by phosphate-buffered saline (PBS) supplemented with 0.1% Triton X-100 for 10 min. Afterward, non-specific binding was blocked with 3% bovine serum albumin (BSA) dissolved in PBS for 1 h at room temperature. Cells were incubated with a primary antibody against SMAD7 (1:100 dilution; R&D; MAB2029) for 1 h at room temperature. After three times of washing with PBS, the specimens were probed with secondary antibodies in a dilution of 1:1000 for 1 h at room temperature. The specimens were then subjected to three washes with PBS and mounted with VECTASHIELD antifade mounting medium with DAPI (Vector Laboratories; H-1200). Experiments were performed three times, and representative results are shown. For F-actin staining, A549 cells were treated without or with TGF-β (2.5 ng/mL) for 48 h and incubated with Phalloidin conjugated with Alexa Fluor 488 (1:500 dilution; Thermo Fisher Scientific; A12379). Experiments were performed twice, and representative results are shown. Images were acquired with a Leica SP8 confocal microscope (Leica Microsystems).

Ubiquitination assay

MDA-MB-231-HA-Ub cells were treated with MG132 (5 µM) for 5 h prior to harvesting. Cells were washed with cold PBS twice containing 10 mM N-ethylmaleimide (NEM; Sigma-Aldrich; E3876), cells were lysed in 1% SDS-RIPA buffer (25 mM Tris–HCl, pH 7.4, 150 mM NaCl, 1% NP40, 0.5% sodium deoxycholate and 1% SDS) consisting of protease inhibitors and 10 mM NEM. Lysates were subsequently boiled for 5 min and diluted to 0.1% SDS at a final concentration in RIPA buffer. Then protein concentrations were measured and the same amount of proteins were incubated with 2 µL TβRI antibody (Abcam; ab235578) for 16 h at 4 °C. The mixture was then incubated with 20 µL of Protein A Sepharose (GE Healthcare; 17-0963-03) for 2 h at 4 °C. After five washes, the beads were boiled in 2× sample buffer and analyzed by western blotting. Experiments were performed three times, and representative images are shown.

Co-immunoprecipitation (Co-IP)

HEK293T transfected with indicated plasmids were lysed with TNE lysis buffer (50 mM Tris–HCl, pH 7.4, 1 mM EDTA, 150 mM NaCl, and 1% NP40) containing freshly added complete protease inhibitor cocktail and kept on ice for 15 min. The lysates were centrifuged at 1.4×10^4 g for 10 min at 4 °C. Equal amounts of protein were incubated with anti-FLAG agarose beads (Sigma–Aldrich; A2220) for 30 min at 4 °C with rotation. Pierce™ Protein G Agarose (Thermo Fisher Scientific; 20397) was added and kept for 2 h at 4 °C with rotation. Beads were washed five times with the TNE buffer for 5 min at 4 °C with rotation. Afterward, samples were boiled with 2× sample buffer for 5 min and subjected to SDS-PAGE analysis.

IncuCyte migration assays

40 µl MDA-MB-231 cells suspended in medium supplemented with 0.5% serum were seeded at a density of 1×10^3 in the inserts of an Incucyte clearview 96-well plate (Essen BioScience; 4582). 20 µl medium supplemented with 0.5% serum-containing indicated compounds or corresponding vehicle controls was added into the inserts. Afterward, cells were allowed to settle at ambient temperature for 20 min. In parallel, 200 µl medium supplemented with 10% serum was added to the reservoir plates. Then the inserts containing cells were placed into a pre-filled plate. Cells on the top and bottom of inserts were imaged and analyzed using the IncuCyte live cell imaging system (Essen BioScience). Cells were treated without or with TGF-β (5 ng/mL) during the assays. To test the effect of JQ-1 on cell migration, cells were treated without or with JQ-1 (1 µM) for 24 h before seeding. Cells in the top and bottom chambers were imaged and quantified with the IncuCyte system. Experiments were performed three times, and representative images are shown.

Subcellular fractionation

Cytoplasmic and nuclear fractions were collected from MDA-MB-231 cells (challenged with or without TGF-β (5 ng/mL) for 1 day or Dox (0.1 μg/mL) for 2 days). Cells were collected and lysed in 250 μl of buffer A (50 mM Tris–HCl (pH 7.4), 150 mM NaCl, 1% NP40, and 0.25% sodium deoxycholate) for 15 min on ice. After centrifugation at 3000 × *g* for 5 min, the supernatant was collected and saved as the cytoplasmic fraction. The pellet was washed with PBS twice and resuspended in 150 μl of buffer B (50 mM Tris–HCl (pH 7.4), 400 mM NaCl, 1% NP40, 0.5% sodium deoxycholate, and 1% SDS). After 20 min of incubation on ice and centrifugation at 12,000 × *g* for 15 min, the supernatant was collected and saved as the nuclear fraction. The isolated cytoplasmic and nuclear fractions were used to quantify the expression of RNA transcripts by RT-qPCR. Experiments were performed three times, and representative results are shown.

RNA immunoprecipitation (RIP)

To identify interactions between *SNAI1e* and BRD4, RIP was performed with a Magna RIP™ RNA-Binding Protein Immunoprecipitation Kit (Merck Millipore; 17-700). Anti-BRD4 antibody (Cell Signaling Technology; 13440), anti-YTHDC1 antibody (Cell Signaling Technology; 77422s), or normal rabbit IgG was incubated with MDA-MB-231 cell lysates for 16 h at 4 °C. For in vitro RIP, 10 pmol of in vitro-transcribed *SNAI1e* was incubated with 2 μg recombinant FLAG-SMURF2 protein (Sigma–Aldrich; SRP0228) or FLAG-BRD4 BD1/2 recombinant protein (R&D systems; SP-600) for 16 h at 4 °C as described previously[21]. RNA was extracted from the beads, and RT–qPCR was performed as mentioned above. Experiments were performed three times, and representative results are shown.

RNA pull-down assay

A MEGAscript Kit (Thermo Fisher Scientific; AM1334) was used for in vitro RNA synthesis. 50 pmol of RNA was biotinylated with an RNA 3′ End Desthiobiotinylation Kit (Thermo Fisher Scientific; 20160). The tertiary structure of each lncRNA was recovered by 10 min of incubation at 70 °C followed by gradual cooling to room temperature. HEK293T cell lysates or FLAG-BRD4 BD1/2 recombinant protein (R&D systems; SP-600) was incubated with biotinylated *LETS1*[22], *SNAI1e-AS* or *SNAI1e* for 16 h at 4 °C. Proteins were eluted from the beads and analyzed by western blotting. Experiments were performed three times, and representative images are shown.

Proximity ligation analysis (PLA)

PLA was performed to analyze the endogenous interaction between SMAD7 and SNAI1. MDA-MB-231 cells were fixed and incubated with primary antibodies against SMAD7 (R&D; MAB2029) and SNAI1 (Cell Signaling Technology; 3879S) at a 1:500 dilution for 16 h at 4 °C. PLUS and MINUS PLA probes conjugated to secondary antibodies (Sigma–Aldrich; DUO92001 and DUO92005) were used to incubate cells for 1 h at 37 °C. Ligase (Sigma–Aldrich; DUO92008) was added to the cells for a 30-min incubation before Duolink® Polymerase (Sigma–Aldrich; DUO82028) incubation for 90 min at 37 °C. Images were acquired with a Leica SP8 confocal microscope (Leica Microsystems). Experiments were performed three times, and representative images are shown.

Flow cytometry

MCF10A-M2 cells were incubated with fluorescein isothiocyanate (FITC)-conjugated anti-human CD44 (BD Biosciences; 347943) and R-phycoerythrin (PE)-conjugated anti-human CD24 (BD Biosciences; 555428) antibodies (1:500 dilution) for 30 min at 37 °C. IgG isotypes (560952/560951; BD Biosciences) were used as a control. At least 10,000 cells were acquired with a BD LSR II flow cytometer (BD Biosciences), and the results were analyzed with FlowJo 10.5.0 software (for gating strategy, see Supplementary Fig. 10). Experiments were performed three times, and representative results are shown.

Tumor sphere formation assays

MCF10A-M2 cells were resuspended in DMEM/F12 medium (no phenol red; Thermo Fisher Scientific; 21041033) containing 1× B27 (Thermo Fisher Scientific; 17504044) and 20 ng/ml EGF (Sigma–Aldrich; 01-107). 2000 cells were seeded into wells of an ultralow attachment 24-well plate (Corning; CLS3473-24EA). To test the effect of JQ-1 on cell stemness, cells were pre-treated without or with JQ-1 (1 μM) for 24 h before seeding. After 14 days of standard incubation, the numbers of spheres (>50 mm diameter) were counted using an inverted microscope (DMi8; Leica Microsystems). Experiments were performed three times, and representative results are shown.

RNA-seq-based transcriptional profiling and GSEA

To screen for mRNAs affected by *SNAI1e*, the DNBSeq platform (BGI, Hong Kong) was used to perform RNA-seq in MDA-MB-231 cells upon CRISPRa-mediated *SNAI1e* overexpression. RNA-seq reads were processed using the opensource BIOWDL RNA-seq pipeline v5.0.0 (https://eur03.safelinks.protection.outlook.com/?url=https%3A%2F%2Fzenodo.org%2Frecord%2F5109461%23.Ya2yLFPMJhE&data=05%7C02%7Cc.fan%40lumc.nl%7C745ef3b26cca4179ad3108dcb5216766%7Cc4048c4fdd544cbd80495457aacd2fb8%7C0%7C0%7C638584402282389605%7CUnknown%7CTWFpbGZsb3d8eyJWIjoiMC4wLjAwMDAiLCJQIjoiV2luMzIiLCJBTiI6Ik1haWwiLCJXVCI6Mn0%3D%7C0%7C%7C%7C&sdata=f%2FKAhFLm%2BzgqqZEAhf0O1ns2ygC5sFlRJAgCXN5qgPs%3D&reserved=0) developed at the LUMC. This pipeline performs FASTQ preprocessing (including quality control, quality trimming, and adapter clipping), alignment, read quantification, and optionally transcript assembly. FastQC (v0.11.9) was used for checking raw read QC. Adapter clipping was performed using Cutadapt (v2.10) with the default settings. RNA-seq reads' alignment was performed using STAR (v2.7.5a) on human reference genome GRCh38. The gene read quantification was performed using HTSeq-count (v0. 12.4) with the Ensembl gene annotation version 111. |Log2(fold change)| >1, false discovery rate <0.05 was set as a cutoff. The upregulated genes upon *SNAI1e* overexpression are listed in Supplementary Data 4. The TGF-β[83], BMP[84], WNT[85] and YAP[86] response gene signature, SNAI1-induced gene signature[87], and EMT (GO: 0001837) gene signature were used to perform GSEA with the GSEA software[85].

Fluorescence in situ hybridization (FISH)

MDA-MB-231 cells were treated without or with TGF-β (5 ng/mL) for 8 h. An RNAScope® Multiplex Fluorescent Kit (Advanced Cell Diagnostics; 323100) was utilized to evaluate the expression and localization of *SNAI1e* in the cells. Images were acquired with a Leica SP8 confocal microscope (Leica Microsystems). Representative results from two independent experiments are shown.

Embryonic zebrafish extravasation assay

The experiments were conducted in a licensed establishment for the breeding and use of experimental animals (LU) and subject to internal regulations and guidelines, stating that advice is taken from the animal welfare body to minimize suffering for all experimental animals housed at the facility. The zebrafish assays described are not considered an animal experiment under the Experiments on Animals Act (Wod, effective 2014), the applicable legislation in the Netherlands in accordance with the European guidelines (EU directive no. 2010/63/EU) regarding the protection of animals used for scientific purposes, because non-self-eating larvae where used. Therefore, no license specific for these assays on zebrafish larvae (<5 days post fertilization) was required. MDA-MB-231 cells labeled with mCherry were injected into the duct of Cuvier of embryos from transgenic zebrafish (*fli*; EGFP) as previously described[33]. Approximately 200 MDA-MB-231 cells were injected in Fig. 2j and Supplementary Fig. 2m, while around 400 MDA-MB-231 cells were injected in Figs. 2k, 7i. Vehicle control (DMSO) or JQ-1 (1 μM) was added to the egg

water from the first day post injection. An inverted SP5 STED confocal microscope (Leica) was used to visualize the injected cancer cells and zebrafish embryos. Two independent experiments were performed, and representative results are shown., zebrafish

Circular chromosome conformation capture (4C) sequencing

4C experiments were performed strictly following a detailed protocol as described elsewhere[43]. Briefly, MDA-MB-231 cells were serum-starved for 16 h and stimulated without or with TGF-β (5 ng/mL) for 24 h. 5×10^6 cells were collected and fixed with 2% formaldehyde for 10 min, followed by quenching with 0.13 M glycine. After cell lysis and nuclei isolation, the samples were digested with 100 U DpnII (New England Biolabs, R0543M) and ligated using 50 U T4 DNA ligase (Thermo Fisher Scientific; EL0012). Next DNA samples were reverse cross-linked and purified by Nucleomag PCR beads (Macherey Nagel; 744100.34). 50 U Csp6I (Thermo Fisher Scientific; ER0211) was added for second digestion, after which the second ligation was performed using 50 U T4 DNA ligase. A 2-step 4C PCR was carried out using viewpoint specific primers for *SNAI1e* (TACACGACGCTCTTCCGATCTTCTGGGCAACAGAGGGAGAT, ACTGGAGTTCAGACGTGTGCTCTTCCGATCTGCTTCAGTCCTCGCTAAGAA) using Expand™ Long Template PCR System (Roche; 11681834001) to prepare the library and add Illumina adapters for sequencing. 4C libraries were sequenced on an Illumina NextSeq 2000 platform. FastQ files were demultiplexed and processed as previously described[41] (https://github.com/deLaatLab/pipe4C). Reads were mapped against hg38. Read counts were normalized to one million mapped intra-chromosomal reads excluding the two highest covered fragments and 21 fragment end rolling mean scores were calculated for every fragment end. Biological replicates ($n = 3$) were averaged, and profile overlays were produced using R 4.2.0 (https://www.R-project.org).

Statistics & reproducibility

Statistical analyses were performed using a two-tailed unpaired Student's t-test, or one/two-way ANOVA with GraphPad Prism 10.2.3 as indicated in the figure legends. Each experiment was repeated independently for two or three times (as indicated in the figure legends and "Methods" section) with similar results. The exact value of n, which represents the number of technical or biological replicates used in the experiments, is indicated in the figure legends. $P < 0.05$ was considered statistically significant. For the number of zebrafish used in the study, sample sizes were determined according to experience with previous experiments[33,88]. Zebrafish isolated from eggs were mixed in one plate containing egg water to randomize them before injection of cells with genetic manipulation. No data points were excluded from the analyses. The investigators were not blinded to allocation during experiments and outcome assessment. All measurements in this study were taken from distinct samples.

Reporting summary

Further information on research design is available in the Nature Portfolio Reporting Summary linked to this article.

Data availability

The CRISPRa screen, 4C-seq, and RNA-seq data generated in this study have been deposited in the GEO database and under accession code GSE276203, GSE274882, and GSE274181, respectively. Source data are provided with this paper.

References

1. Nieto, M. A., Huang, R. Y., Jackson, R. A. & Thiery, J. P. EMT: 2016. *Cell* **166**, 21–45 (2016).
2. Pastushenko, I. & Blanpain, C. EMT transition states during tumor progression and metastasis. *Trends Cell Biol.* **29**, 212–226 (2019).
3. Brabletz, T., Kalluri, R., Nieto, M. A. & Weinberg, R. A. EMT in cancer. *Nat. Rev. Cancer* **18**, 128–134 (2018).
4. Fan, C., Zhang, J., Hua, W. & ten Dijke, P. Biphasic role of TGF-β in cancer progression: from tumor suppressor to tumor promotor. In *Reference Module in Biomedical Sciences* (Elsevier, 2018).
5. ten Dijke, P., Miyazono, K., Heldin, C. H. & Moustakas, A. Special issue: TGF-β and epithelial-mesenchymal transition in cancer. *Semin. Cancer Biol.* **102-103**, 1–3 (2024).
6. Liu, S., Ren, J. & ten Dijke, P. Targeting TGFβ signal transduction for cancer therapy. *Signal Transduct. Target Ther.* **6**, 8 (2021).
7. Katsuno, Y. et al. Chronic TGF-β exposure drives stabilized EMT, tumor stemness, and cancer drug resistance with vulnerability to bitopic mTOR inhibition. *Sci. Signal.* **12**, eaau8544 (2019).
8. Tzavlaki, K. & Moustakas, A. TGF-β Signaling. *Biomolecules* **10**, 487 (2020).
9. Massagué, J. & Sheppard, D. TGF-β signaling in health and disease. *Cell* **186**, 4007–4037 (2023).
10. Yan, X., Xiong, X. & Chen, Y. G. Feedback regulation of TGF-β signaling. *Acta Biochim. Biophys. Sin. (Shanghai)* **50**, 37–50 (2018).
11. Liu, J., Jin, J., Liang, T. & Feng, X. H. To Ub or not to Ub: a regulatory question in TGF-β signaling. *Trends Biochem. Sci.* **47**, 1059–1072 (2022).
12. Kavsak, P. et al. Smad7 binds to Smurf2 to form an E3 ubiquitin ligase that targets the TGFβ receptor for degradation. *Mol. Cell* **6**, 1365–1375 (2000).
13. Ebisawa, T. et al. Smurf1 interacts with transforming growth factor-β type I receptor through Smad7 and induces receptor degradation. *J. Biol. Chem.* **276**, 12477–12480 (2001).
14. Nakao, A. et al. Identification of Smad7, a TGFβ-inducible antagonist of TGF-β signalling. *Nature* **389**, 631–635 (1997).
15. Mattick, J. S. et al. Long non-coding RNAs: definitions, functions, challenges and recommendations. *Nat. Rev. Mol. Cell Biol.* **24**, 430–447 (2023).
16. Palazzo, A. F. & Koonin, E. V. Functional long non-coding RNAs evolve from junk transcripts. *Cell* **183**, 1151–1161 (2020).
17. Herman, A. B., Tsitsipatis, D. & Gorospe, M. Integrated lncRNA function upon genomic and epigenomic regulation. *Mol. Cell* **82**, 2252–2266 (2022).
18. Hou, T. Y. & Kraus, W. L. Spirits in the material world: enhancer RNAs in transcriptional regulation. *Trends Biochem. Sci.* **46**, 138–153 (2021).
19. Sartorelli, V. & Lauberth, S. M. Enhancer RNAs are an important regulatory layer of the epigenome. *Nat. Struct. Mol. Biol.* **27**, 521–528 (2020).
20. Kumar, D. B. U. et al. A genome-wide CRISPR activation screen identifies a novel super-enhancer demarcated by eRNAs. *Front. Mol. Biosci.* **10**, 1110445 (2023).
21. Fan, C. et al. LncRNA *LITATS1* suppresses TGF-β-induced EMT and cancer cell plasticity by potentiating TβRI degradation. *EMBO J.* **42**, e112806 (2023).
22. Fan, C. et al. The lncRNA *LETS1* promotes TGF-β-induced EMT and cancer cell migration by transcriptionally activating a TβR1-stabilizing mechanism. *Sci. Signal.* **16**, eadf1947 (2023).
23. Rodrigues-Junior, D. M. & Moustakas, A. Unboxing the network among long non-coding RNAs and TGF-beta signaling in cancer. *Ups. J. Med. Sci.* **129**, e10614 (2024).
24. Konermann, S. et al. Genome-scale transcriptional activation by an engineered CRISPR-Cas9 complex. *Nature* **517**, 583–588 (2015).
25. Papoutsoglou, P. & Moustakas, A. Long non-coding RNAs and TGF-β signaling in cancer. *Cancer Sci.* **111**, 2672–2681 (2020).
26. Marvin, D. L. et al. Dynamic Visualization of TGF-β/SMAD3 transcriptional responses in single living cells. *Cancers* **14**, 2508 (2022).
27. Lizio, M. FANTOM Consortium et al. Gateways to the FANTOM5 promoter level mammalian expression atlas. *Genome Biol.* **16**, 22 (2015).

28. Abugessaisa, I. et al. FANTOM5 CAGE profiles of human and mouse reprocessed for GRCh38 and GRCm38 genome assemblies. *Sci. Data* **4**, 170107 (2017).
29. Volders, P. J. et al. LNCipedia: a database for annotated human lncRNA transcript sequences and structures. *Nucleic Acids Res.* **41**, D246–D251 (2013).
30. Fang, S. et al. NONCODEV5: a comprehensive annotation database for long non-coding RNAs. *Nucleic Acids Res.* **46**, D308–D314 (2018).
31. Wang, L. et al. CPAT: coding-potential assessment tool using an alignment-free logistic regression model. *Nucleic Acids Res.* **41**, e74 (2013).
32. Genome Atlas, Cancer et al. The Cancer Genome Atlas Pan-Cancer analysis project. *Nat. Genet.* **45**, 1113–1120 (2013).
33. Ren, J., Liu, S., Cui, C. & ten Dijke, P. Invasive behavior of human breast cancer cells in embryonic zebrafish. *J. Vis. Exp.* **122**, 55459 (2017).
34. Gilbert, L. A. et al. CRISPR-mediated modular RNA-guided regulation of transcription in eukaryotes. *Cell* **154**, 442–451 (2013).
35. Wilson, M. M., Weinberg, R. A., Lees, J. A. & Guen, V. J. Emerging mechanisms by which EMT programs control stemness. *Trends Cancer* **6**, 775–780 (2020).
36. Kim, B. N. et al. TGF-β induced EMT and stemness characteristics are associated with epigenetic regulation in lung cancer. *Sci. Rep.* **10**, 10597 (2020).
37. Al-Hajj, M., Wicha, M. S., Benito-Hernandez, A., Morrison, S. J. & Clarke, M. F. Prospective identification of tumorigenic breast cancer cells. *Proc. Natl Acad. Sci. USA* **100**, 3983–3988 (2003).
38. Konermann, S. et al. Transcriptome engineering with RNA-targeting type VI-D CRISPR effectors. *Cell* **173**, 665–676 (2018).
39. Halder, S. K., Beauchamp, R. D. & Datta, P. K. A specific inhibitor of TGF-β receptor kinase, SB-431542, as a potent antitumor agent for human cancers. *Neoplasia* **7**, 509–521 (2005).
40. Tsirigoti, C., Ali, M. M., Maturi, V., Heldin, C. H. & Moustakas, A. Loss of SNAI1 induces cellular plasticity in invasive triple-negative breast cancer cells. *Cell Death Dis.* **13**, 832 (2022).
41. Dhasarathy, A., Phadke, D., Mav, D., Shah, R. R. & Wade, P. A. The transcription factors Snail and Slug activate the transforming growth factor-β signaling pathway in breast cancer. *PLoS ONE* **6**, e26514 (2011).
42. Vincent, T. et al. A SNAIL1-SMAD3/4 transcriptional repressor complex promotes TGF-β mediated epithelial-mesenchymal transition. *Nat. Cell Biol.* **11**, 943–950 (2009).
43. Krijger, P. H. L., Geeven, G., Bianchi, V., Hilvering, C. R. E. & de Laat, W. 4C-seq from beginning to end: A detailed protocol for sample preparation and data analysis. *Methods* **170**, 17–32 (2020).
44. Kang, Y., Kim, Y. W., Kang, J. & Kim, A. Histone H3K4me1 and H3K27ac play roles in nucleosome eviction and eRNA transcription, respectively, at enhancers. *FASEB J.* **35**, e21781 (2021).
45. Creyghton, M. P. et al. Histone H3K27ac separates active from poised enhancers and predicts developmental state. *Proc. Natl Acad. Sci. USA* **107**, 21931–21936 (2010).
46. Kubo, N. et al. H3K4me1 facilitates promoter-enhancer interactions and gene activation during embryonic stem cell differentiation. *Mol. Cell* **84**, 1742–1752 (2024).
47. Lauberth, S. M. et al. H3K4me3 interactions with TAF3 regulate preinitiation complex assembly and selective gene activation. *Cell* **152**, 1021–1036 (2013).
48. Wang, H. et al. H3K4me3 regulates RNA polymerase II promoter-proximal pause-release. *Nature* **615**, 339–348 (2023).
49. Shechner, D. M., Hacisuleyman, E., Younger, S. T. & Rinn, J. L. Multiplexable, locus-specific targeting of long RNAs with CRISPR-display. *Nat. Methods* **12**, 664–670 (2015).
50. Rahnamoun, H. et al. RNAs interact with BRD4 to promote enhanced chromatin engagement and transcription activation. *Nat. Struct. Mol. Biol.* **25**, 687–697 (2018).
51. Kanno, T. et al. BRD4 assists elongation of both coding and enhancer RNAs by interacting with acetylated histones. *Nat. Struct. Mol. Biol.* **21**, 1047–1057 (2014).
52. Liang, Y., Tian, J. Y. & Wu, T. BRD4 in physiology and pathology: "BET" on its partners. *Bioessays* **43**, e2100180 (2021).
53. Filippakopoulos, P. et al. Selective inhibition of BET bromodomains. *Nature* **468**, 1067–1073 (2010).
54. Dong, B. & Wu, Y. D. Epigenetic regulation and post-translational modifications of SNAI1 in cancer metastasis. *Int. J. Mol. Sci.* **22**, 11062 (2021).
55. Hoot, K. E. et al. Keratinocyte-specific Smad2 ablation results in increased epithelial-mesenchymal transition during skin cancer formation and progression. *J. Clin. Invest.* **118**, 2722–2732 (2008).
56. Cho, H. J., Baek, K. E., Saika, S., Jeong, M. J. & Yoo, J. Snail is required for transforming growth factor-β-induced epithelial-mesenchymal transition by activating PI3 kinase/Akt signal pathway. *Biochem. Biophys. Res. Commun.* **353**, 337–343 (2007).
57. Lee, J. H. et al. TGF-β and RAS jointly unmask primed enhancers to drive metastasis. *Cell* **187**, 6182–6199 (2024).
58. Wang, Y. et al. The emerging role of super enhancer-derived non-coding RNAs in human cancer. *Theranostics* **10**, 11049–11062 (2020).
59. Li, R. et al. Super-enhancer RNA m(6)A promotes local chromatin accessibility and oncogene transcription in pancreatic ductal adenocarcinoma. *Nat. Genet.* **55**, 2224–2234 (2023).
60. Lennox, K. A. & Behlke, M. A. Cellular localization of long non-coding RNAs affects silencing by RNAi more than by antisense oligonucleotides. *Nucleic Acids Res.* **44**, 863–877 (2016).
61. Wu, H. et al. Tissue-specific RNA expression marks distant-acting developmental enhancers. *PLoS Genet.* **10**, e1004610 (2014).
62. Zhang, Z. et al. HeRA: an atlas of enhancer RNAs across human tissues. *Nucleic Acids Res.* **49**, D932–D938 (2021).
63. Lu, L. et al. Inhibition of BRD4 suppresses the malignancy of breast cancer cells via regulation of Snail. *Cell Death Differ.* **27**, 255–268 (2020).
64. Qin, Z. Y. et al. BRD4 promotes gastric cancer progression and metastasis through acetylation-dependent stabilization of snail. *Cancer Res.* **79**, 4869–4881 (2019).
65. Zaware, N. & Zhou, M. M. Bromodomain biology and drug discovery. *Nat. Struct. Mol. Biol.* **26**, 870–879 (2019).
66. Miller, T. C. et al. A bromodomain-DNA interaction facilitates acetylation-dependent bivalent nucleosome recognition by the BET protein BRDT. *Nat. Commun.* **7**, 13855 (2016).
67. Morrison, E. A. et al. DNA binding drives the association of BRG1/hBRM bromodomains with nucleosomes. *Nat. Commun.* **8**, 16080 (2017).
68. Hu, W., Qin, L., Li, M., Pu, X. & Guo, Y. A structural dissection of protein-RNA interactions based on different RNA base areas of interfaces. *RSC Adv.* **8**, 10582–10592 (2018).
69. Sanchez de Groot, N. et al. RNA structure drives interaction with proteins. *Nat. Commun.* **10**, 3246 (2019).
70. Kishore, S. et al. A quantitative analysis of CLIP methods for identifying binding sites of RNA-binding proteins. *Nat. Methods* **8**, 559–564 (2011).
71. Booth, B. J. et al. RNA editing: expanding the potential of RNA therapeutics. *Mol. Ther.* **31**, 1533–1549 (2023).
72. Birgaoanu, M., Sachse, M. & Gatsiou, A. RNA editing therapeutics: advances, challenges and perspectives on combating heart disease. *Cardiovasc. Drugs Ther.* **37**, 401–411 (2023).
73. Devaiah, B. N. et al. BRD4 is a histone acetyltransferase that evicts nucleosomes from chromatin. *Nat. Struct. Mol. Biol.* **23**, 540–548 (2016).
74. Dey, A. et al. BRD4 directs hematopoietic stem cell development and modulates macrophage inflammatory responses. *EMBO J.* **38**, e100293 (2019).

75. Mele, D. A. et al. BET bromodomain inhibition suppresses T17-mediated pathology. *J. Exp. Med.* **210**, 2181–2190 (2013).
76. Tang, P., Zhang, J. F., Liu, J., Chiang, C. M. & Ouyang, L. Targeting bromodomain and extraterminal proteins for drug discovery: from current progress to technological development. *J. Med. Chem.* **64**, 2419–2435 (2021).
77. Asangani, I. A. et al. Therapeutic targeting of BET bromodomain proteins in castration-resistant prostate cancer. *Nature* **510**, 278–282 (2014).
78. Stratikopoulos, E. E. et al. Kinase and BET inhibitors together clamp inhibition of PI3K signaling and overcome resistance to therapy. *Cancer Cell* **27**, 837–851 (2015).
79. Doench, J. G. et al. Optimized sgRNA design to maximize activity and minimize off-target effects of CRISPR-Cas9. *Nat. Biotechnol.* **34**, 184–191 (2016).
80. Sanson, K. R. et al. Optimized libraries for CRISPR-Cas9 genetic screens with multiple modalities. *Nat. Commun.* **9**, 5416 (2018).
81. Schmierer, B. et al. CRISPR/Cas9 screening using unique molecular identifiers. *Mol. Syst. Biol.* **13**, 945 (2017).
82. Li, W. et al. MAGeCK enables robust identification of essential genes from genome-scale CRISPR/Cas9 knockout screens. *Genome Biol.* **15**, 554 (2014).
83. Padua, D. et al. TGFβ primes breast tumors for lung metastasis seeding through angiopoietin-like 4. *Cell* **133**, 66–77 (2008).
84. Pangas, S. A. et al. Conditional deletion of Smad1 and Smad5 in somatic cells of male and female gonads leads to metastatic tumor development in mice. *Mol. Cell Biol.* **28**, 248–257 (2008).
85. Subramanian, A. et al. Gene set enrichment analysis: a knowledge-based approach for interpreting genome-wide expression profiles. *Proc. Natl Acad. Sci. USA* **102**, 15545–15550 (2005).
86. Zhang, J., Smolen, G. A. & Haber, D. A. Negative regulation of YAP by LATS1 underscores evolutionary conservation of the Drosophila Hippo pathway. *Cancer Res.* **68**, 2789–2794 (2008).
87. Carmichael, C. L. et al. The EMT modulator SNAI1 contributes to AML pathogenesis via its interaction with LSD1. *Blood* **136**, 957–973 (2020).
88. Ren, J. et al. Reactivation of BMP signaling by suboptimal concentrations of MEK inhibitor and FK506 reduces organ-specific breast cancer metastasis. *Cancer Lett.* **493**, 41–54 (2020).

Acknowledgements

The results here are in part based upon data generated by the TCGA Research Network (https://www.cancer.gov/tcga). This study was supported by ZonMW grant (09120012010061) to P.t.D. Part of this work was carried out at the CRISPR Functional Genomics unit funded by SciLifeLab to B.S. We acknowledge support from the National Genomics Infrastructure, the National Academic Infrastructure for Supercomputing in Sweden (NAISS), partially funded by the Swedish Research Council through grant agreement no. 2022-06725, and the Uppsala Multidisciplinary Center for Advanced Computational Science (UPPMAX) to B.S.

Author contributions

C.F.: Conceptualization; investigation; methodology; writing – original draft; writing – review and editing. Q.W.: Conceptualization; supervision; investigation; methodology; writing – original draft; writing – review and editing. P.H.L.K.: Investigation; methodology. D.C.: Investigation; methodology. M.S.: Investigation. O.K.: Investigation. S.D.: Investigation. B.S.: Investigation; methodology. H.M.: Investigation; methodology. W.d.L.: Investigation; methodology. P.t.D.: Conceptualization; supervision; writing – original draft; project administration; writing – review and editing.

Competing interests

The authors declare no competing interests.

Additional information

Supplementary information The online version contains supplementary material available at https://doi.org/10.1038/s41467-025-58032-w.

Correspondence and requests for materials should be addressed to Qian Wang or Peter ten Dijke.

Peer review information *Nature Communications* thanks Sven Diederichs and the other, anonymous, reviewer(s) for their contribution to the peer review of this work. A peer review file is available.